Review | Open Access

Energy Z

Jeong *et al. Energy Z* **2026**, *2*, 200013 **DOI:**10.20517/energyz.2026.19

Dry-processed thick electrodes for high-energy-density lithium-sulfur batteries

Yun Ho Jeong[1,#], Gyuri Jung[2,#], Changshin Jo[1,2,*]

Keywords:
Lithium-sulfur battery, thick electrode, dry process

Citation: Jeong, Y. H.; Jung, G.; Jo, C. Dry-processed thick electrodes for high-energy-density lithium-sulfur batteries. *Energy Z* **2026**, *2*, 200013. https://dx.doi.org/10.20517/energyz.2026.19

Received: 19 Apr 2026
First Decision: 13 May 2026
Revised: 1 Jun 2026
Accepted: 15 Jun 2026
Published: 2 Jul 2026

Academic Editor:
Yuping Wu
Copy Editor:
Shu-Yuan Duan
Production Editor:
Shu-Yuan Duan

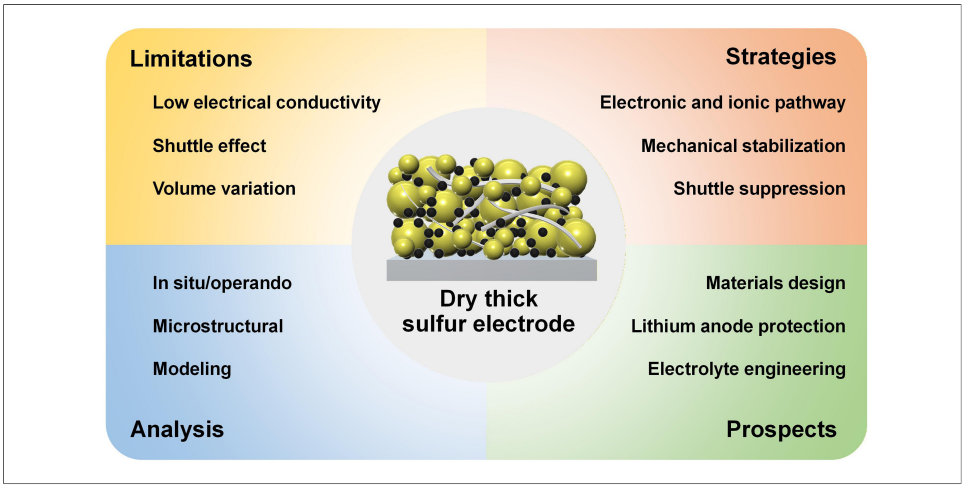

Abstract

Lithium-sulfur batteries (LSBs) have attracted significant attention as next-generation high-energy-density storage systems owing to the high theoretical capacity of sulfur, its natural abundance, and low cost. However, the practical realization of cell-level energy density remains challenging due to intrinsic limitations, including the low electrical conductivity of active material, the polysulfide shuttle phenomenon, and large volume changes. To achieve practical high-energy density, thick sulfur cathodes with high sulfur loading are required. In thick electrodes, limitations in electronic and ionic transport, reaction inhomogeneity, and structural instability become more pronounced. Dry electrode processes are emerging as a promising alternative for designing thick LSB electrodes, as they can overcome the structural limitations of wet-based processes while enabling high electrode density and more uniform conductive networks. This review provides a systematic overview of design strategies for dry thick LSB electrodes and discusses approaches to mitigate key performance-limiting factors. Furthermore, reaction mechanisms and transport phenomena are analyzed through *in situ/operando* characterization, and design directions for the realization of practical high-energy-density cells are proposed. This review aims to facilitate the development of practical

[1]Department of Chemical Engineering, Pohang University of Science and Technology (POSTECH), Pohang 37673, Republic of Korea.
[2]Department of Battery Engineering, Graduate Institute of Ferrous & Eco Materials Technology (GIFT), Pohang University of Science and Technology (POSTECH), Pohang 37673, Republic of Korea.
[#]These authors contributed equally to this work.

[*]**Correspondence to:** Prof. Changshin Jo, Department of Battery Engineering, Graduate Institute of Ferrous & Eco Materials Technology (GIFT), Pohang University of Science and Technology (POSTECH), Pohang 37673, Republic of Korea. E-mail: jochangshin@postech.ac.kr

high-energy-density LSBs by outlining structural design principles and research directions in dry thick-electrode technologies.

INTRODUCTION

With the growing demand for high-energy-density storage in electric vehicles, large-scale energy storage systems (ESS), aerospace and defense applications, there is an increasing need for next-generation rechargeable battery systems beyond conventional lithium-ion batteries. The Battery500 Consortium aims to develop lithium-metal batteries with targets of 500 Wh kg^{-1} energy density, 1,000 charge-discharge cycles, and a cost of US$100 per kWh[1,2]. Among the promising candidates to meet these requirements, lithium-sulfur batteries (LSBs) have attracted considerable attention. LSBs are next-generation rechargeable battery systems that operate via conversion reactions, in which energy is stored through electrochemical reactions between a lithium metal anode and a sulfur cathode ($16Li + S_8 \leftrightarrow 8Li_2S$)[3-8]. During the discharge process, two distinct voltage plateaus are observed at approximately 2.3 V and 2.1 V. In the higher voltage plateau region, elemental sulfur is reduced to long-chain lithium polysulfides (LiPS; Li_2S_n, $4 \leq n \leq 8$), which are subsequently converted into short-chain species such as Li_2S_2 and ultimately into the final discharge product, Li_2S, in the lower voltage plateau region [Figure 1A][9-11]. This multistep reaction involves a total of 16 electrons, allowing sulfur to theoretically deliver a high specific capacity of 1,672 mA h g^{-1} and an exceptionally high theoretical energy density of approximately 2,600 Wh kg^{-1}. In addition, sulfur is abundant, low-cost, and environmentally benign, making LSBs attractive as cost-effective and sustainable next-generation energy storage systems [Figure 1B][12-14].

However, despite their high theoretical capacity and energy density potential, LSBs inherently involve sulfur-based conversion reactions accompanied by several intrinsic limitations [Figure 1C][10,15]. First, sulfur and Li_2S are intrinsically electronically insulating, which limits electron transport within the electrode. This necessitates the incorporation of a high content of conductive agents in the electrode, thereby reducing the active material fraction and compromising the practical energy density at the cell level. Second, LiPSs, which are intermediate species formed during the conversion reaction, are soluble in liquid electrolytes and can migrate between the cathode and anode, inducing the shuttle effect. As a result, continuous loss of active material occurs, accompanied by low coulombic efficiency and rapid capacity fading, thereby deteriorating long-term cycling stability[16]. Third, the conversion of sulfur to Li_2S involves a large volume change of approximately 80%, which can induce electrode cracking or mechanical degradation during repeated charge-discharge cycles, weakening the electrical connectivity within the electrode. Lastly, since most LSBs employ lithium metal as the anode, issues such as lithium dendrite growth, unstable solid-electrolyte interphase (SEI) formation, and reduction of shuttled polysulfides can occur during cycling[17-19]. Such anode instability significantly compromises both safety and long-term cycle life, indicating that stabilization strategies for both the cathode and anode are required for the practical implementation of LSBs.

These limitations degrade electrode performance and become even more pronounced in thick electrode configurations. As electrode thickness increases, the transport pathways for electrons and ions become longer, and for LSB active materials with low conductivity, this hinders conversion reactions and increases reaction inhomogeneity within the electrode. In addition, repeated large volume changes in thick electrodes further aggravate mechanical degradation within the electrode structure. These combined factors significantly limit active material utilization in high-loading and thick electrodes, making the realization of thick electrodes inherently challenging in LSB systems.

In addition to these transport and mechanical issues, increased sulfur loading also raises the areal current density at a given C-rate. This imposes more severe demands on charge transport, reaction kinetics, heat generation, and interfacial stability at the full-cell level. In pouch-type cells, higher areal current can amplify

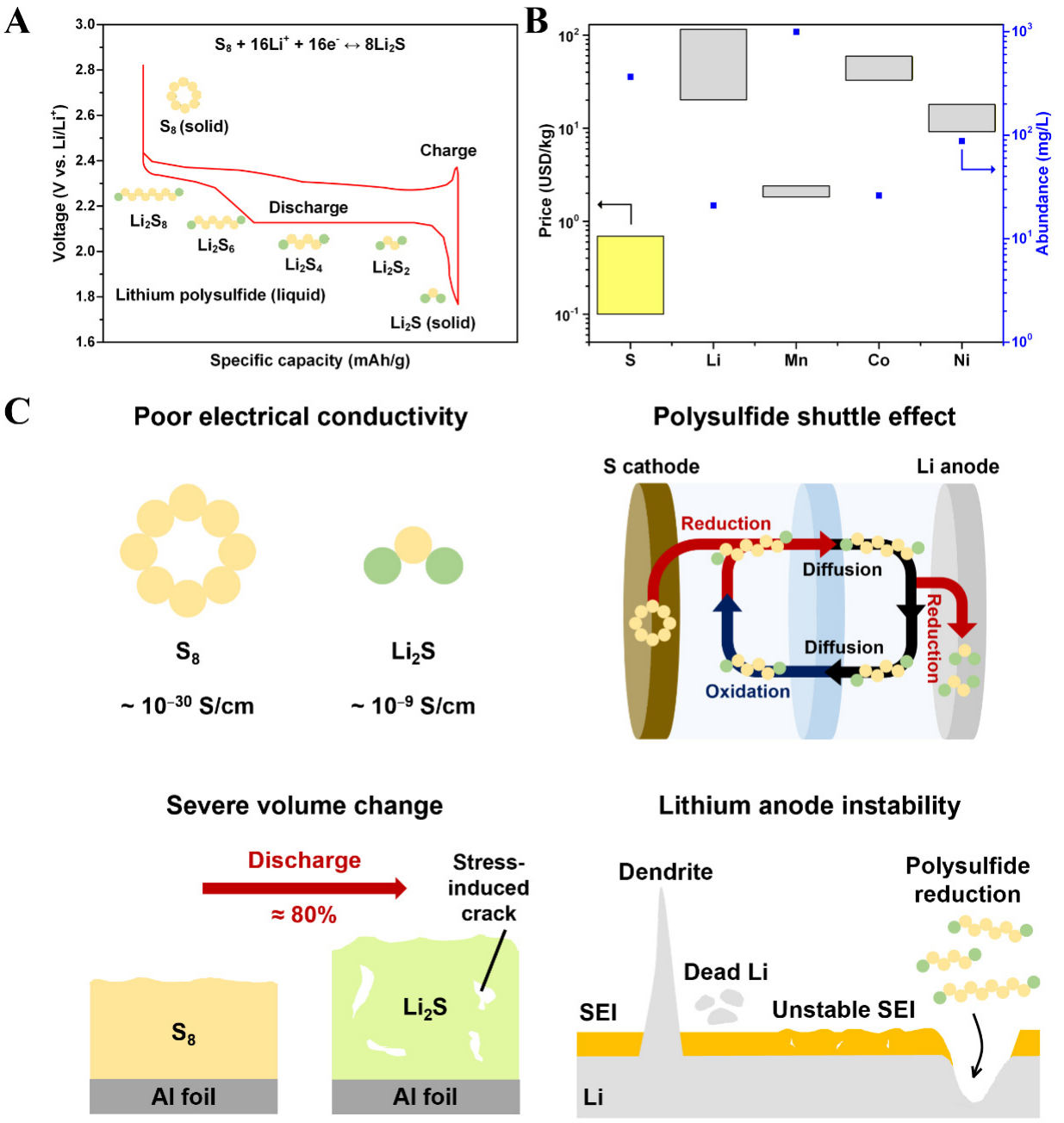

Figure 1. (A) Charge-discharge mechanism of LSBs in liquid organic electrolytes and corresponding voltage profile; (B) Price (including fluctuations over the past decade) and natural abundance of S, Li, Mn, Co, and Ni. The data were obtained from Ref.[12-14]; (C) Schematic illustration of the intrinsic limitations of LSB systems. SEI: Solid-electrolyte interphase; LSB: lithium-sulfur battery.

local polarization and current-density gradients, particularly near tabs, current collectors, and electrode edges, leading to non-uniform reaction distribution and accelerated degradation[20-22]. From the perspective of the lithium metal anode, thick sulfur cathodes require a larger amount of Li stripping/plating per unit area, and the increased areal current density can intensify non-uniform Li flux, pit formation, mossy/dead Li accumulation, SEI instability, and electrolyte consumption[23]. Therefore, a thick-sulfur cathode design should be considered in conjunction with current-collector and tab designs, thermal management, and lithium-metal stabilization to achieve stable high-loading LSB cells.

Beyond the intrinsic limitations of sulfur, the energy density achieved by LSBs at the practical cell level remains below expectations[22,24,25]. In particular, for applications with stringent weight and volume constraints, maximizing energy density at the cell and system levels is essential. Recent studies analyzing energy density and key design parameters have shown that the practical energy density of LSBs is not solely determined by the theoretical capacity of sulfur but is strongly influenced by multiple design parameters, including sulfur loading, sulfur utilization, electrolyte-to-sulfur ratio (E/S ratio), and negative-to-positive capacity ratio (N/P ratio)[2,5]. The gravimetric energy density of LSBs was estimated using a formulation that separates practical energy-density losses into mass-related and energy-output-related contributions. In this approach, the theoretical energy density of an LSB is corrected by two factors: R_{weight} and R_{energy}. R_{weight} represents the fraction of electrochemically active materials relative to the total cell mass, reflecting the mass penalty from inactive components such as current collectors, separator, electrolyte, excess lithium, and packaging. R_{energy} describes the practically accessible energy output, which is determined by the sulfur-specific capacity and the average discharge voltage. The theoretical energy density of an LSB, 2,567 Wh kg^{-1}, was used as the baseline value, and the practical gravimetric energy density was calculated as follows:

$$\text{Energy density} = 2,567\ \text{Wh kg}^{-1} \times R_{weight} \times R_{energy} \tag{1}$$

$$R_{energy} = \frac{C_{sulfur}}{1675\text{mAh g}^{-1}} \times \frac{V_{cathode}}{2.2\ \text{V}} \tag{2}$$

In Equation (2), C_{sulfur} is the specific discharge capacity of sulfur and $V_{cathode}$ is the average discharge voltage of the cell.

$$R_{weight} = \frac{\frac{M_{Li_2S}}{M_S} \times m_{sl} \times \left(1 - R_{package}\right)}{\frac{m_{sl}}{R_{cathode}} + \frac{m_{Al}+m_{Cu}}{2} + m_{separator} + \rho_E \times R_{E/S} \times m_{sl} + \frac{2M_{Li}}{M_S} \times R_{N/P} \times m_{sl}} \tag{3}$$

In Equation (3), M_{Li2S}, M_S, and M_{Li} are the molar masses of Li_2S, S, and Li, respectively, with values of 45.947, 32.065, and 6.941 g mol^{-1}. The symbol m_{sl} denotes the areal mass loading of sulfur in the cathode, while $R_{package}$ represents the package-to-total-cell mass ratio and was set to 10% in this calculation. $R_{cathode}$ is the sulfur mass fraction in the cathode. The symbols m_{Al}, m_{Cu}, and $m_{separator}$ denote the areal masses of the aluminum current collector, copper current collector, and separator. Since Li metal can be used without a Cu current collector, m_{Cu} was excluded in this calculation. The areal masses of the 10 μm Al current collector and separator were set to 2.7 and 1.0 mg cm^{-2}, respectively. The symbol ρ_E denotes the electrolyte density and was set to 1.1 g mL^{-1}. $R_{E/S}$ and $R_{N/P}$ represent the E/S ratio and N/P ratio, respectively.

Using the energy density formulation described above, we compared various cell-parameter combinations and generated the analysis plots shown in [Figure 2A-C]. These results indicate that lowering the E/S ratio is one of the most effective ways to increase cell-level energy density [Figure 2A]. However, excessively lean electrolyte conditions can cause insufficient electrode wetting, sluggish ion transport, and continuous electrolyte consumption through side reactions, which limit their practical implementation. In this regard, increasing sulfur loading provides a more direct and practical route to reduce the relative contribution of inactive components, and the effect of sulfur loading on energy density becomes more pronounced under lean-electrolyte conditions. Nevertheless, higher sulfur loading is not always beneficial, because excessive electrode thickness can decrease sulfur utilization and capacity. Therefore, the optimal sulfur loading must be determined by considering sulfur utilization together with cell-level energy density. The calculation also shows that high-energy density can, in principle, be achieved even at relatively low sulfur loading if inactive

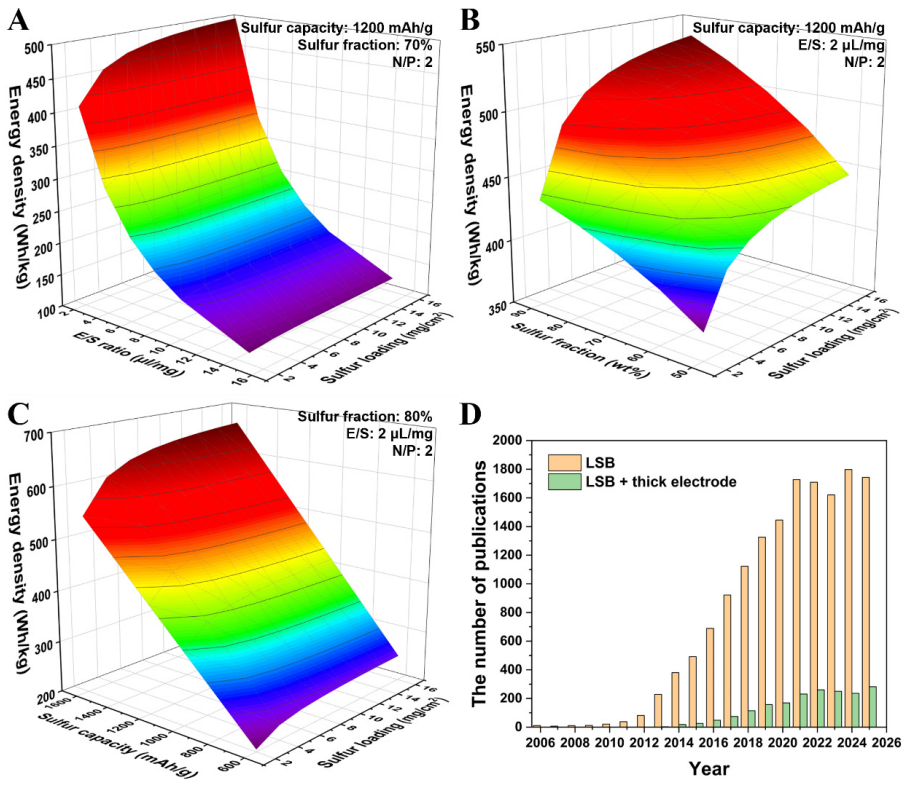

Figure 2. (A) Cell-level energy density in pouch cells as a function of E/S ratio and sulfur loading (sulfur capacity = 1,200 mAh g^{-1}, sulfur fraction = 70%, N/P ratio = 2); (B) Cell-level energy density in pouch cells as a function of sulfur fraction and sulfur loading (sulfur capacity = 1,200 mAh g^{-1}, E/S ratio = 2 μL mg^{-1}, N/P ratio = 2); (C) Cell-level energy density in pouch cells as a function of sulfur capacity and sulfur loading (sulfur fraction = 80%, E/S ratio = 2 μL mg^{-1}, N/P ratio = 2). The calculations in (A-C) were performed based on the energy density formulation reported in Ref.[2]; (D) Approximate number of publications over the past 20 years based on keyword searches. "LSB" corresponds to publications identified using the keywords "Li-S battery," "Li-S batteries," "lithium-sulfur battery," or "lithium-sulfur batteries," while "LSB + thick electrode" corresponds to publications identified using the keywords "thick electrode," "thick electrodes," "high sulfur loading," "high areal loading," or "high mass loading." Data source: Web of Science. LSB: Lithium-sulfur battery; E/S: electrolyte-to-sulfur; N/P:

components are minimized and cell parameters such as E/S and N/P ratios are simultaneously optimized. However, most representative lithium-sulfur pouch cells reporting energy densities above 400 Wh kg^{-1} have still employed high sulfur loadings, highlighting the practical importance of high-loading electrode design[26-29]. Therefore, although sulfur loading alone does not determine the final cell-level energy density, increasing sulfur loading remains an important and practical strategy for reducing inactive mass contribution and realizing high-energy-density LSBs under realistic cell configurations.

In addition, both the sulfur fraction and sulfur loading within the electrode exhibit a strong correlation with electrode energy density. As the loading increases from low to high, the energy density increases steeply [Figure 2B]. This trend highlights the importance of reducing the proportion of inactive components, such as conductive additives and binders, and designing a more densely packed electrode structure to enhance energy density. However, the intrinsically low electrical conductivity of sulfur becomes a major limitation at high loading. Thick electrodes exhibit higher ionic and electronic transport resistance and non-uniform electrochemical reactions along the electrode depth, which limit sulfur utilization. Therefore, to achieve high-energy-density LSBs, electrode design strategies that enhance sulfur conversion kinetics and enable uniform redox reactions throughout the electrode are required [Figure 2C]. Overall, these results highlight that achieving practical high-energy-density LSBs requires thick sulfur cathodes that simultaneously enable high loading and sulfur utilization while maintaining low E/S and N/P ratios.

However, studies on thick electrodes in LSBs over the past two decades remain relatively limited, with a significant portion still focusing on laboratory-scale evaluations under low sulfur loading conditions [Figure 2D]. Since the Nazar group reported carbon host-based sulfur cathodes in 2009, research on LSBs has expanded rapidly, with early studies primarily focusing on addressing intrinsic challenges, such as low electrical conductivity, the polysulfide shuttle phenomenon, and poor cycling stability, as well as fundamental electrochemical behavior[30-32]. As LSB research has progressed, understanding of reaction mechanisms and design parameters at the system level has deepened, leading to greater emphasis on key design variables for practical applications. In particular, the importance of high sulfur loading for achieving meaningful improvements in cell-level energy density is now widely recognized. In line with this trend, research on thick sulfur cathodes has gained increasing attention since the mid-2010s.

This review provides a comprehensive overview of recent advances in dry thick LSB electrodes and systematically organizes strategies for achieving practically viable high-energy-density and stable thick LSB systems. First, the concept and fabrication methods of dry electrodes are introduced, followed by an in-depth discussion of key requirements for thick LSB electrodes, including electronic and ionic transport, mechanical stabilization, and suppression of the polysulfide shuttle, based on previous studies in this field. Furthermore, *in situ* and *operando* characterization techniques for understanding the structural evolution and reaction behavior of dry thick LSB electrodes are summarized, and future research directions for precise design and mechanism-based optimization are proposed. This review aims to establish rational design principles and guide the development of application-oriented research strategies, thereby facilitating the practical realization of high-energy-density LSBs.

DRY-PROCESSED THICK SULFUR ELECTRODES

Achieving both high-energy density and cost competitiveness is a key challenge not only for current lithium-ion batteries (LIBs) but also for next-generation battery systems. In this context, thick electrodes can increase the amount of active material per unit area and reduce the relative proportion of inactive components, thereby increasing energy density [Figure 3A]. In addition, thick electrodes can reduce the electrode area and the number of stacked cells required to achieve a given cell capacity, thereby providing additional benefits such as reduced current collector usage, simplified packaging, and lower manufacturing costs[33,34]. These benefits are particularly important in applications such as electric vehicles and ESS, which require large-area electrodes.

Currently, slurry-based wet coating processes are widely used as the standard method for electrode fabrication in commercial LIBs and in most LSB studies. In a typical wet process, active materials, conductive additives, and binders are dispersed in an organic solvent to form a slurry, which is then coated onto a current collector and dried to produce the electrode. This process has been widely adopted in commercial production due to its high reproducibility. However, when electrode loading is increased to fabricate thick electrodes, wet coating processes exhibit several structural and processing limitations [Figure 3B][35,36]. First, when thick electrodes are fabricated via wet coating, if the thickness exceeds the critical cracking threshold, internal stresses generated during drying can induce cracks on the electrode surface or weaken adhesion to the current collector, leading to delamination[37]. Such cracking not only degrades the mechanical stability of the electrode but also disrupts conductive pathways, leading to degraded electrochemical performance. Moreover, even in electrodes that appear crack-free, solvent evaporation during drying can cause migration of slurry components, leading to the redistribution of binders and conductive additives along the electrode thickness[38]. This compositional inhomogeneity results in non-uniform electronic conduction networks and ionic transport pathways within thick electrodes, leading to spatially non-uniform electrochemical reactions. In addition, thick electrodes fabricated via wet processes generally exhibit high porosity and low electrode density. These structural characteristics increase the amount of electrolyte required to fill the electrode pore

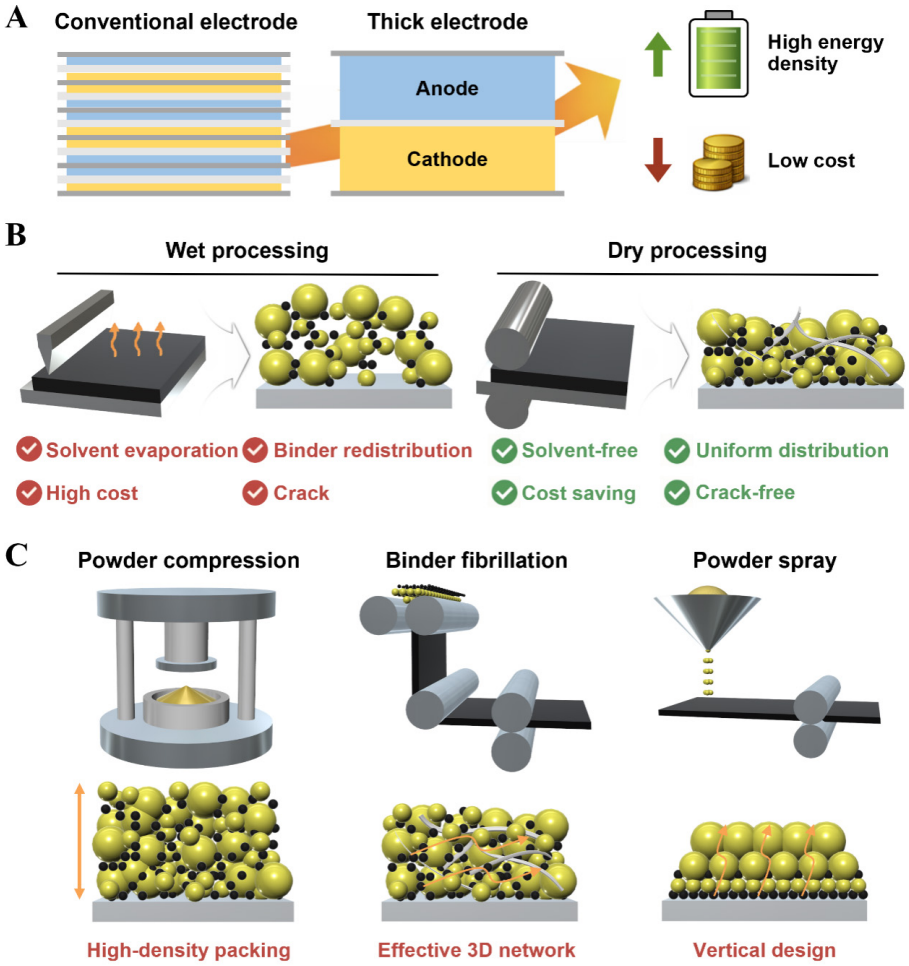

Figure 3. (A) Schematic comparison of conventional and thick electrodes; (B) Comparison of wet processing and dry processing methods, along with the resulting electrode structures; (C) Representative dry electrode fabrication methods, including powder compression, binder fibrillation, and powder spray, and the corresponding electrode structures.

volume. In systems such as LSBs, where the electrolyte serves as the reaction medium, leading to a higher E/S ratio, ultimately lowering the cell-level energy density. From a processing perspective, wet coating also has several drawbacks. The organic solvents used in slurry preparation require substantial time and energy for drying and recovery[39,40]. For LSB cathodes, the drying step may introduce additional risks, including sulfur sublimation and incomplete solvent removal. This issue becomes particularly critical when aqueous slurries are used, as residual water can deteriorate cell performance owing to the high moisture sensitivity of lithium metal and the associated polysulfide/electrolyte chemistry. Furthermore, the use of solvents introduces environmental burdens and safety concerns, underscoring the need for environmentally friendly and energy-efficient next-generation electrode fabrication processes.

For these reasons, dry electrode processes have emerged as an alternative to conventional wet processing. These processes form electrodes by directly mixing active materials, conductive additives, and binders without solvents, thereby mitigating structural issues associated with thick electrode fabrication, simplifying the manufacturing process, and reducing costs. In addition, the absence of a drying step suppresses the migration of binders and conductive additives within the electrode, enabling a more uniform compositional distribution and more continuous electronic conduction networks. Furthermore, this approach can facilitate the fabrication of electrodes with higher density and lower porosity, potentially reducing electrolyte consumption and improving cell-level energy density. Importantly, the improved structural stability and

reaction uniformity of dry-processed thick sulfur cathodes may also influence the behavior of the Li metal anode. In slurry-processed thick sulfur cathodes, cathode cracking, structural degradation, and loss of electronic contact can lead to spatially non-uniform sulfur utilization. The resulting uneven Li-ion flux and local current-density distribution can promote non-uniform Li stripping/plating at the Li metal surface, accelerating mossy/dead Li formation, SEI instability, and continuous electrolyte consumption. In contrast, dry-processed thick sulfur cathodes with improved mechanical integrity and more uniform electronic contact may promote more homogeneous cathode reactions, thereby reducing Li-ion flux localization and contributing to improved Li metal anode stability[41]. Overall, dry electrode processes represent a promising manufacturing strategy for next-generation high-energy-density batteries[42,43].

Dry electrode fabrication methods developed to date can be broadly categorized into three main approaches, each with distinct characteristics in terms of microstructure formation and mechanical binding mechanisms [Figure 3C]. First, the powder compression method is the simplest form of dry processing, in which active materials and conductive additives are uniformly mixed, with or without a binder, and subsequently compressed to form the electrode structure[44]. This approach offers advantages in process simplification and cost reduction. In particular, the compression process effectively reduces interparticle spacing, enabling high electrode density and low porosity, which are beneficial for thick electrode fabrication. However, because interparticle contact is pressure-dependent, the conductive network within the electrode may become non-uniform depending on the pressure distribution, and localized stress may lead to microcrack formation. Therefore, achieving both high electrode density and uniform conductive pathways with structural stability requires precise control over compression pressure and particle size distribution. In addition, its limited compatibility with roll-to-roll processing presents a challenge for commercialization.

Second, the binder fibrillation method involves mixing polymer binders with active materials and conductive additives, followed by shear-induced fibrillation to form a three-dimensional network. Polytetrafluoroethylene (PTFE) is commonly used as the binder because its high molecular weight, linear structure, and weak interchain interactions enable fibrillation under sufficient shear force[45]. As a result, binder fibrillation is among the most promising approaches for industrial applications in dry electrode technologies, owing to its capability for precise thickness control, low energy consumption, and compatibility with roll-to-roll processing. Recent studies have focused on optimizing binder content, controlling mixing conditions to maximize fibrillation efficiency, and developing new binder systems[46-48].

Third, the powder spray method forms electrodes by directly spraying dry powder materials onto the current collector surface, followed by calendering to consolidate the electrode layer. This approach is well suited for continuous processing and large-area electrode fabrication. In addition, direct powder spraying offers flexibility in controlling the through-thickness composition of the electrode, enabling the fabrication of gradient or multilayer structures. However, achieving reproducible electrode thickness and composition requires precise control over powder characteristics and spray/deposition conditions, such as particle size, spray rate, and substrate temperature, as well as subsequent compression conditions[49,50].

Overall, dry electrode fabrication methods differ in their structure formation mechanisms and therefore exhibit distinct characteristics in terms of mechanical stability, conductive network formation, and scalability. These differences become particularly important in thick electrode applications, where high electrode density, continuous conductive pathways, and structural integrity during repeated cycling must be achieved concurrently. Therefore, tailored design strategies that account for the unique characteristics of each fabrication method are essential.

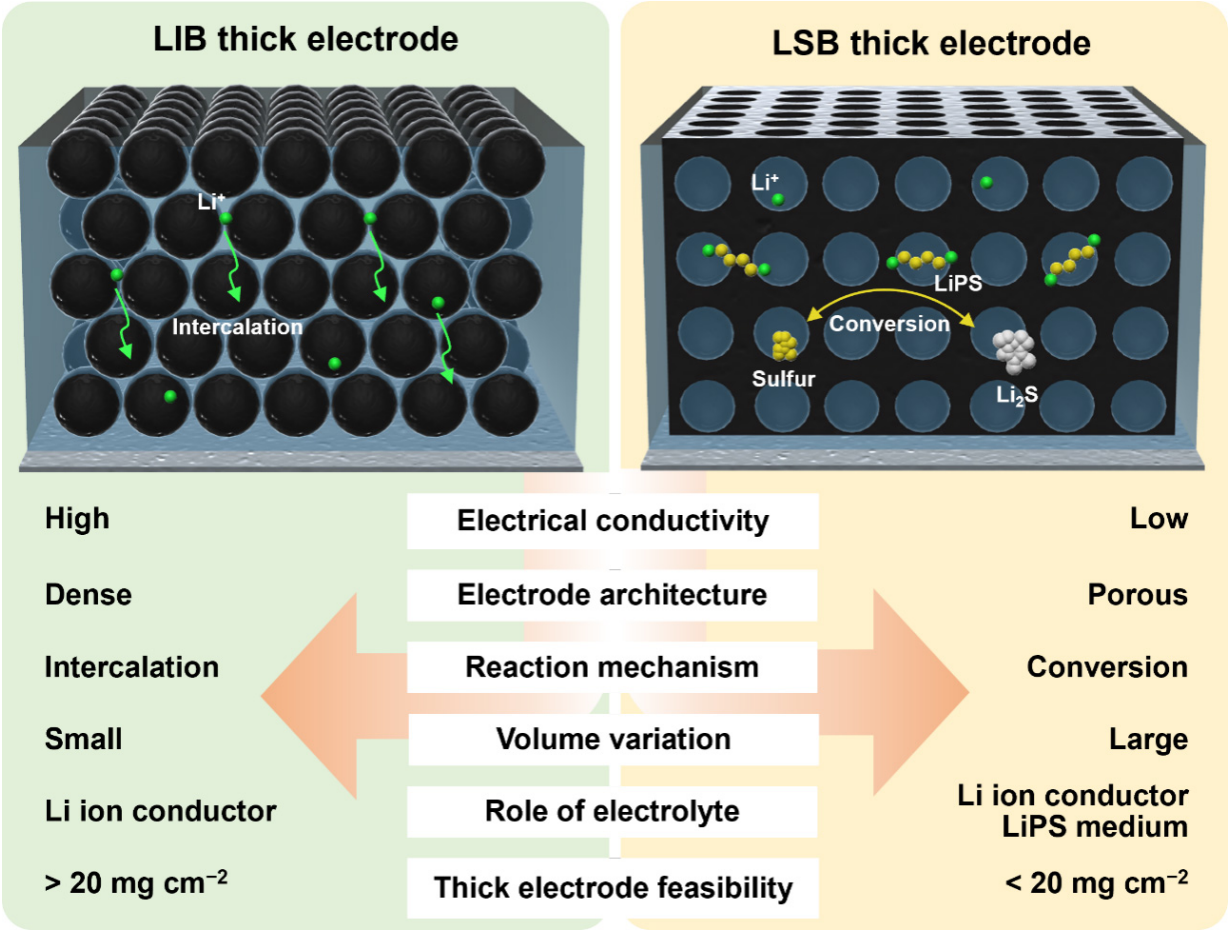

Figure 4. Comparison of LIB and LSB systems under thick electrode conditions. LIB: Lithium-ion battery; LSB: Lithium-sulfur battery.

Despite these advantages and design opportunities, the practical implementation of thick electrodes remains challenging. As electrode thickness increases, maintaining structural uniformity and mechanical integrity during fabrication becomes more difficult. Even when thick electrodes are successfully fabricated, longer ion and electron transport pathways lead to increased transport resistance and reaction heterogeneity along the electrode depth, resulting in poor active material utilization and unstable long-term cycling performance[36]. These limitations are more pronounced in LSB systems than in LIB systems, largely because the active material properties and reaction mechanisms in LSBs differ fundamentally from those in LIBs [Figure 4].

From a materials perspective, sulfur and Li_2S have intrinsically low electrical conductivity and are often incorporated as small particles within conductive carbon hosts or sulfur/carbon composites in LSB electrodes[51]. As a result, a high content of conductive additives is required to establish sufficient electron transport pathways. However, increasing the conductive additive content reduces the active material fraction and limits the achievable energy density of thick electrodes[52,53]. In contrast, many conventional LIB cathode materials are composed of micron-sized secondary particles, typically on the order of 10 μm or larger, and generally exhibit higher electrical conductivity than sulfur and Li_2S[54,55]. Therefore, LIB electrodes can achieve sufficient conductive networks with lower carbon content and form denser electrode structures with lower porosity, making them more suitable for achieving high volumetric energy density.

Conventional liquid-electrolyte LSBs based on elemental sulfur operate via sulfur conversion reactions accompanied by dissolution and precipitation processes[56]. During cycling, soluble LiPS species dissolve into the electrolyte and migrate through the porous electrode, leading to concentration gradients and reaction

heterogeneity along the electrode thickness. These issues become more pronounced in thick electrodes, where Li_2S may precipitate preferentially in certain regions while sulfur remains underutilized in others. In addition, the large volume change between sulfur and Li_2S during repeated cycling can induce cracks, delamination, and contact loss, further compromising electrode integrity. In contrast, LIB cathodes primarily operate through Li-ion intercalation reactions within solid particles. As a result, compositional and phase changes are largely confined within solid particles, and the associated volume changes are generally smaller, facilitating structural stability during cycling.

These differences in reaction mechanisms also lead to different roles of the electrolyte and electrode architecture. In liquid-electrolyte LSBs, the electrolyte acts not only as a medium for Li-ion transport but also as a reaction medium due to the repeated dissolution, migration, and precipitation of LiPSs. This can lead to accumulation of LiPS species, changes in electrolyte transport properties, formation of concentration gradients, and deterioration of reaction kinetics. In contrast, in LIBs, the electrolyte primarily functions as a Li-ion transport medium and interfacial component, and its role is less directly coupled to the active-material reaction than in liquid-electrolyte LSBs.

However, these considerations should be distinguished from other LSB configurations in which polysulfide dissolution is partially or substantially suppressed. In sulfurized polyacrylonitrile (SPAN)-based cathodes, sulfur is chemically confined within a polyacrylonitrile (PAN)-derived framework, which mitigates soluble polysulfide formation and shifts the key design focus toward sulfur utilization, reaction kinetics, electrode conductivity, and interfacial stability[57]. In all-solid-state LSBs (ASSLSBs), the use of solid-state electrolytes substantially suppresses polysulfide dissolution and shuttling, but introduces different limitations associated with solid-solid interfacial contact, continuous ionic/electronic pathways, triple-phase contact, and mechanical degradation during sulfur/Li_2S conversion[58]. Therefore, the effects of areal loading and thick-electrode design should be evaluated according to the dominant sulfur reaction pathway and the electrolyte configuration.

Overall, LIB thick electrodes have been reported with active-material loadings exceeding 20 mg cm^{-2} while maintaining relatively stable intercalation-based reaction mechanisms and electrode structures. In contrast, in conventional liquid-electrolyte LSBs, the combination of low electronic conductivity, reaction inhomogeneity, structural instability, and strong electrolyte dependence at high sulfur loading makes thick-electrode design significantly more challenging.

DRY-PROCESSING STRATEGIES TO ADDRESS THE LIMITATIONS OF THICK SULFUR CATHODES

This section discusses dry-processing-based design strategies to address key challenges in thick LSB electrodes, including limited electronic and ionic transport, large volume changes, and the polysulfide shuttle effect. Given the fundamental differences in material properties and reaction mechanisms between LIB and LSB systems, the loading regime relevant to thick-electrode design differs substantially between the two systems. While LIB thick electrodes often employ active-material loadings exceeding 20 mg cm^{-2}[59], LSB electrodes can exhibit pronounced transport limitations, reaction heterogeneity, and electrolyte-dependent behavior even at much lower sulfur loadings because of the low conductivity of sulfur/Li_2S and the dissolution-precipitation nature of polysulfide chemistry. In this context, sulfur loadings of 4 mg cm^{-2} or higher are commonly regarded in high-energy and high-loading LSB studies as a practically relevant regime, where areal capacity, electrolyte wetting, LiPS transport, and Li metal utilization become critical design factors[5,25]. Therefore, in this review, dry thick sulfur cathodes are operationally defined as electrodes with sulfur loadings of 4 mg cm^{-2} or higher, and relevant studies are discussed based on this definition [Table 1].

Table 1. Summary of reported dry-processed thick lithium-sulfur electrodes, including design strategies to overcome the limitations of thick sulfur cathodes, electrode parameters, and electrochemical performance

Strategy	Method	AM	Loading mass (mg cm^{-2})	AM fraction (%)	Electrolyte composition	E/S ratio (μL mg^{-1})	Specific capacity(mAh g^{-1})	Areal capacity (mAh cm^{-2})	Pouch cell	Ref
Electronic and ionic transport	Binder fibrillation	Li_2S	3.5-4	68-78	1 M LiTFSI, 0.25 M $LiNO_3$ in DME/DOL (1:1 v/v) 1 M LiTFSI, 0.125 M $LiNO_3$, 0.125 M Li_2S_6 in DME/DOL (1:1 v/v)	4.8-5.5 (E/AM)	800-1,300 (0.1C) 500-700 (0.1C, 100 cycle)	2.9-3.4	X	[60]
		Sulfur	3-4.85	63.75	1 M LiTFSI, 0.25 M $LiNO_3$ in DME/DOL (1:1 v/v)	6.8	1,000-1,300 (0.1C) 900-1,000 (0.1C, 80 cycle)	2.4-5.82	X	[61]
		Sulfur	7	30	S:LPSCl:AB = 30:50:20 wt%	SSE	1,314 (0.05C) 1,140.6 (0.05C, 140 cycle)	11	X	[62]
		Li_2S	4.3	30	LPSCl:acrylate binder = 98:2 wt%	SSE	1,077 (0.33C) 932.7 (0.33C, 50 cycle)	4.5	O (15 mAh)	[62]
		Se-SPAN	5-64.2	80-95	1 M $LiPF_6$, 10 wt% FEC in EC/DEC/DMC (1:1:1 v/v/v)	5 (E/AM)	614.6 (0.2 A g^{-1}) 580.1 (0.2 A g^{-1}, 100 cycle)	5.4-31	X	[63]
		Se-SPAN	12	80-95	1 M $LiPF_6$, 10 wt% FEC in EC/DEC/DMC (1:1:1 v/v/v)	5 (E/AM)	583 (0.05 A g^{-1}) 550 (0.05 A g^{-1}, 20 cycle)	7	O (40 mAh)	[63]
		Sulfur	4.5	66.7	1 M LiTFSI, 0.25 M $LiNO_3$ in DME/DOL (1:1 v/v)	14.4	1,125 (0.1C)	5.1	X	[64]
		SPAN	10	80	1M $LiPF_6$, 0.05 M LiDFOB in EMC/FEC (3:1 v/v)	12	~ 1,200 (0.25C) ~ 948 (0.25C, 300 cycle)	11	X	[65]
	Powder compression	SPAN	5	80	1M $LiPF_6$, 0.05 M LiDFOB in EMC/FEC (3:1 v/v)	12	~ 1,200 (0.5C) ~829.2 (0.5C, 150 cycle)	6	O (90 mAh)	[65]
		Sulfur	15.6	77	1 M LiTFSI, 0.2 M $LiNO_3$ in DME/DOL (1:1 v/v)	6.7	1,270 (0.025C)	19.8	X	[66]
		Sulfur	5.72-7.01	47.5	1 M LiTFSI, 0.2 M $LiNO_3$ in DME/DOL (1:1 v/v)		1,316 (~ 0.03C)	~10	X	[67]
		Sulfur	5.9	60	LPB glass-ceramic argyrodite	SSE	999.7 (0.1C)	5.9	X	[68]
		Sulfur	12	64	1 M LiTFSI, 0.25 M $LiNO_3$ in DME/DOL (1:1 v/v)	6	833 (0.033C) ~ 666 (0.033C, 50 cycle)	10	X	[41]
Mechanical stabilization	Binder fibrillation	Sulfur	14	64	1 M LiTFSI, 0.25 M $LiNO_3$ in DME/DOL (1:1 v/v)	4.5	857 (0.033C) ~ 571 (0.033C, 40 cycle)	12	O (122 mAh)	[41]
		Li_2S	10	64	1 M LiTFSI, 0.25 M $LiNO_3$ in DME/DOL (1:1 v/v)	6 (E/AM)	881 (0.033C) 520 (0.033C, 50 cycle)	8.81	X	[41]
		Sulfur	4.5	40	LiSiPSCl/PTFE composite	SSE	1,512.2 (0.2C) 1,067.4 (0.2C, 30 cycle)	6.8	X	[69]

Shuttle suppression	Binder fibrillation	Sulfur	12.5	63	1 M LiTFSI, 2 wt% $LiNO_3$ in DME/DOL (1:1 v/v)		966 (0.2C) 850.1 (0.2C, 100 cycle)	12.1	X	[70]
		Sulfur	18.6	63	1 M LiTFSI, 2 wt% $LiNO_3$ in DME/DOL (1:1 v/v)	5.3	763 (0.1C) 618 (0.1C, 50 cycle)	14.2	O (N/A)	[70]
		Sulfur	3.5-3.8	64	1 M LiTFSI, 0.25 M $LiNO_3$ in DME/DOL (1:1 v/v)	4	972 (0.1C) 794 (0.1C, 50 cycle)	2.9	X	[71]
	Powder compression	Sulfur	4.31-4.46	25	1 M LiTFSI, 0.2 M $LiNO_3$ in DME/DOL (1:1 v/v)	7	1,509 (0.03C) 500 (0.03C, 100 cycle)	6.74	X	[72]

AM: Active material; E: electrolyte; SSE: solid-state electrolyte; LiTFSI: lithium bis(trifluoromethanesulfonyl)imide; DME: 1,2-dimethoxyethane; DOL: 1,3-dioxolane; LPSCl: lithium phosphorus sulfur chloride; AB: acetylene black; FEC: fluoroethylene carbonate; EC: ethylene carbonate; DEC: diethyl carbonate; DMC: dimethyl carbonate; LiDFOB: lithium difluoro(oxalate)borate; EMC: ethyl methyl carbonate; LPB: Li_3PS_4-2$LiBH_4$; LiSiPSCl: $Li_{10}Si_{0.3}PS_{6.7}Cl_{1.8}$.

Meanwhile, although powder spraying is a promising dry-processing method for continuous electrode fabrication and through-thickness structural design, reports on its application to dry-processed thick sulfur cathodes remain limited to the best of our knowledge. Accordingly, this review mainly focuses on binder fibrillation and powder compression approaches, for which relevant LSB studies have been reported.

Electronic & ionic transport engineering

In thick LSB electrodes, the intrinsically low electrical conductivity of the active materials severely limits electron transport. In addition, insufficient Li-ion transport pathways can cause reaction heterogeneity and the formation of inactive regions within the electrode depth[25,73]. To address these issues, various strategies have been proposed for dry thick sulfur electrodes, including improving the continuity of conductive networks and precise control of pore structures and electrolyte accessibility to facilitate both electronic and ionic transport.

In binder fibrillation-based electrodes, Kohl *et al.* proposed a strategy to mitigate reaction heterogeneity in thick electrodes by reducing particle size to enhance interfacial reaction kinetics [Figure 5A][60]. By controlling the ball milling time of Li_2SO_4 precursors, Li_2S nanoparticles approximately 50-100 nm in size were synthesized and used as the active material. Li_2S exhibits a high kinetic barrier, which limits the initial oxidation reaction, making the improvement of activation kinetics critical for electrochemical performance[74,75]. Reducing the particle size of Li_2S increases the specific surface area, thereby enlarging the contact area with the electrolyte and promoting interfacial charge-transfer reactions. This is reflected in a capacity difference of approximately 170 mAh g^{-1}, corresponding to about 30% of the total capacity, between electrodes prepared under 4 h and 60 h ball milling conditions. This improvement is attributed to enhanced initial activation of Li_2S nanoparticles. Using this approach, Li_2S electrodes with loadings of 3.5-4 mg cm^{-2} exhibited a high capacity of up to 1,360 mAh g^{-1} at 0.1 C and stable cycling over more than 50 cycles, with a gradual capacity decay of approximately 0.19% per cycle[60]. These results demonstrate that particle-size reduction is an effective strategy for improving interfacial reaction kinetics and enhancing active-material utilization in thick electrode design. However, this study was conducted under conditions of relatively low Li_2S loading and a high E/S ratio, which do not fully reflect practical high-loading and lean-electrolyte conditions.

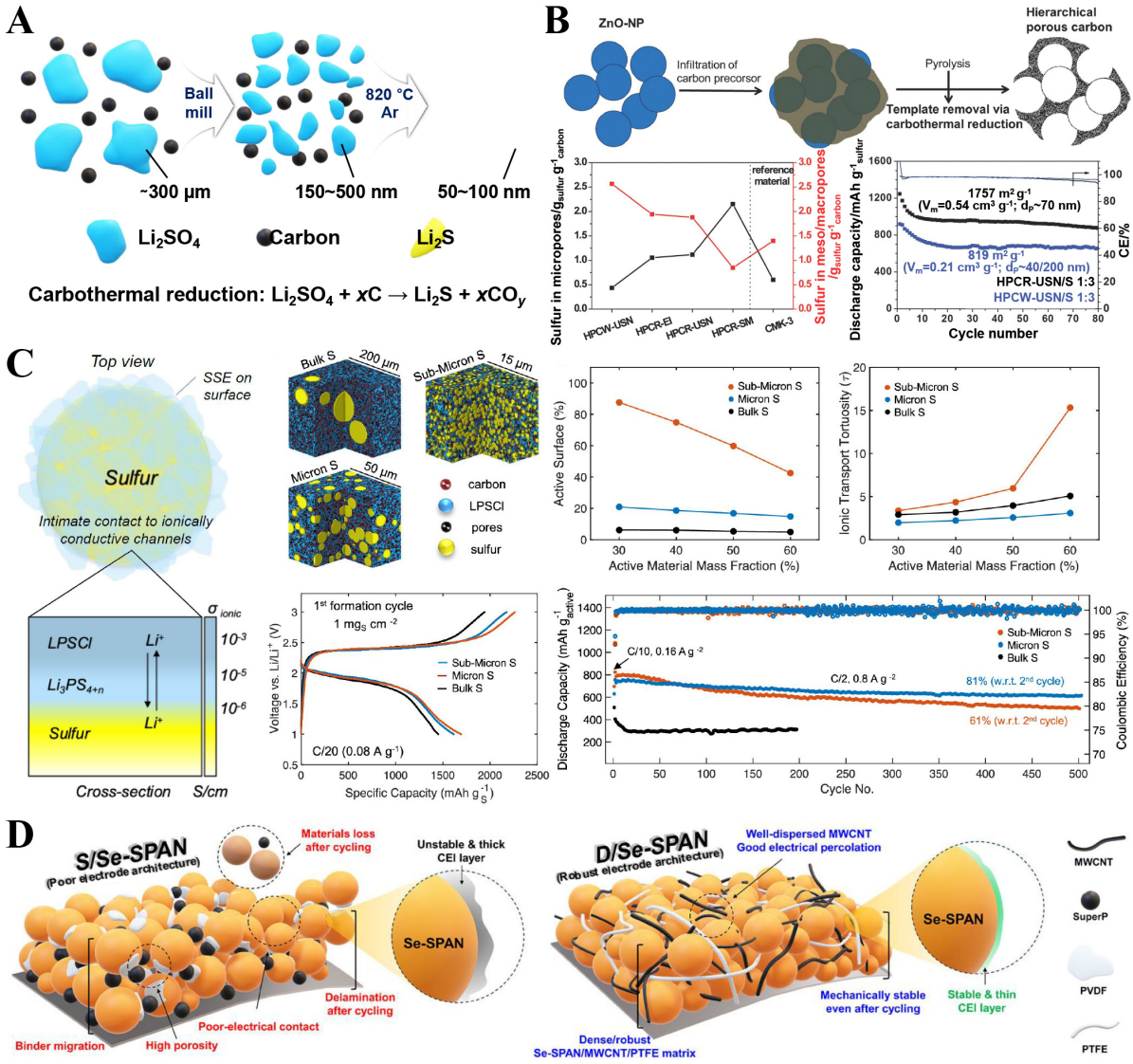

Figure 5. Representative studies of electronic and ionic transport engineering in dry electrodes fabricated by binder fibrillation. (A) Schematic illustration of Li_2S/C composite formation via ball milling-assisted carbothermal reduction of Li_2SO_4 with carbon, based on the processing conditions and particle-size ranges reported in Ref.[60]; (B) Schematic illustration of the formation of hierarchical porous carbon via ZnO hard templating and comparison of sulfur distribution and electrochemical performance depending on pore structure. Adapted with permission from Ref.[61] Copyright © 2014 WILEY-VCH Verlag GmbH & Co. KGaA, Weinheim; (C) Schematic illustration of ionically conductive interphase formation at the sulfur-LPSCl interface (left) and comparison of electrode structure and ionic transport tortuosity as a function of sulfur particle size (right). Reprinted from Ref.[62], under CC BY 4.0 license; (D) Schematic comparison of electrode structure and conductive network formation between wet-processed and dry-processed electrodes. Reprinted from Ref.[63], under CC BY 4.0 license. NP: Nanoparticle; SSE: solid-state electrolyte; LPSCl: lithium phosphorus sulfur chloride; SPAN: sulfurized polyacrylonitrile; MWCNT: multi-walled carbon nanotube; PVDF: poly(vinylidene fluoride); PTFE: polytetrafluoroethylene.

Meanwhile, Strubel *et al.* employed a ZnO hard-templating approach to construct hierarchical porous carbon as a sulfur host, thereby establishing effective charge transport pathways in thick electrodes [Figure 5B][61]. ZnO nanoparticles were employed as sacrificial templates to generate hierarchical porous carbon structures containing micro-, meso-, and macropores, as similarly reported in previous hard-templating studies[61,76]. This hierarchical pore structure provides continuous pathways for electrolyte diffusion and Li-ion transport within the electrode, while also maintaining electronic conduction through the carbon framework. The resulting electrode exhibited improved capacity and stable cycling performance, demonstrating mitigation of transport limitations in thick electrodes. These results highlight the critical role of pore structure in ionic transport and its applicability to dry thick sulfur cathodes. However, since this

study was evaluated at relatively low sulfur loadings and a relatively high E/S ratio of approximately 7 μL mg^{-1}, further validation is required to assess its applicability under practical high-loading and lean electrolyte conditions.

In liquid electrolyte systems, the electrolyte infiltrates the electrode pores and forms continuous ionic transport pathways, enabling relatively efficient Li-ion transport[77]. In contrast, in solid-state electrolyte systems, ionic transport relies on interparticle contact, making the formation of continuous ionic pathways more challenging and rendering ionic transport a dominant limiting factor[78]. Cronk *et al.* proposed two design strategies to simultaneously overcome interfacial and structural limitations that hinder ionic transport and reaction uniformity in sulfide-based Li_6PS_5Cl (LPSCl) ASSLSBs [Figure 5C][62]. First, a mechanochemical one-step milling process was employed to achieve uniform dispersion of sulfur, LPSCl, and carbon, thereby forming intimate triple-phase contact. The resulting structure enhances Li-ion transport within the electrode while enabling efficient electronic conduction. In particular, mechanochemical reactions between sulfur and LPSCl lead to the formation of ionically conductive intermediate phases, such as lithium polysulfidophosphate (Li_3PS_{4+n}), on the sulfur surface[79]. In addition, the amorphous structure formed during milling alters the bonding environment of sulfur, reducing the activation energy for conversion reactions and enabling high sulfur utilization. The resulting electrode exhibited a high discharge capacity of approximately 1,615 mAh g^{-1} and a coulombic efficiency of 128%, which is attributed in part to the redox activity of LPSCl. Furthermore, electrodes using Li_2S as the active material also demonstrated a high capacity of approximately 723 mAh g^{-1} and excellent reversibility of 99.3%, confirming that the interfacial structure effectively promotes Li_2S activation. Second, the authors controlled the particle size of the sulfur active material in the cathode composite. The sulfur particle size was varied from the bulk scale (25-50 μm) to the micron scale (0.5-5 μm), and further to the submicron scale (0.25-0.5 μm). A decrease in particle size increased the active surface area and improved sulfur utilization. In particular, the submicron sulfur electrode exhibited the highest initial capacity of 1,694 mAh g^{-1}, which is attributed to enhanced redox activity of LPSCl due to the increased surface area. However, excessively small particle sizes can increase ionic transport tortuosity and induce chemomechanical stress associated with volume changes during lithiation, leading to the collapse of ionic pathways and interfacial degradation. Indeed, despite superior initial performance, the submicron electrode retained only about 61% of its capacity after 500 cycles, whereas the micron-sized electrode exhibited a higher capacity retention of approximately 81%. Structural design plays a critical role in ASSLSBs, requiring a balance between active surface area, ionic transport, and chemomechanical stability. Notably, the high capacity and coulombic efficiency approaching the theoretical limit of sulfur are partially influenced by the redox activity of the LPSCl electrolyte, and thus the intrinsic utilization of sulfur should be interpreted separately.

Kim *et al.* investigated the effect of PTFE binder fibrillation on transport properties in dry-processed electrodes by comparing electrodes with identical compositions fabricated via wet process and dry process [Figure 5D][63]. In electrodes fabricated via the dry process, fibrillation forms a three-dimensional interconnected network of active material, conductive carbon, and binder, thereby establishing continuous electron-transport pathways throughout the electrode. In contrast, in wet-processed electrodes, dissolved binders can redistribute during slurry drying and form localized coating layers on particle surfaces, which may interrupt direct particle-to-particle contact and reduce the continuity of the conductive network[80]. The fibrillated structure helps maintain the pore architecture within the electrode, facilitating electrolyte infiltration and providing ionic transport pathways, which are particularly important under high-loading conditions. Notably, stable electrode structure and electrochemical performance were achieved even at a high areal sulfur loading of up to approximately 64.2 mg cm^{-2}. Under high-loading conditions, dry electrodes exhibited reduced cracking and improved capacity and cycling performance compared to wet electrodes[63]. These results demonstrate that electrode structure formation via fibrillation can improve transport behavior

within the electrode and lead to enhanced performance. However, it should be noted that different conductive additives were used in the dry and wet electrodes in this study, and thus the influence of conductive additive type should also be considered.

In powder compression-based electrodes, Horst *et al.* compared electronic and ionic transport characteristics arising from differences in electrode structure and interparticle contact states as a function of particle properties and electrode fabrication conditions[64]. In this study, a thermal step was introduced during the powder compression process to induce melt infiltration of sulfur into the carbon matrix on an expanded metal current collector, thereby producing sulfur-carbon black composite powders[81]. This process improved interparticle contact and enabled the formation of a conductive network without a binder. Higher mixing intensity led to sulfur refinement and more uniform carbon dispersion, enhancing electronic conduction pathways. However, excessive mixing or high bulk density reduced porosity, thereby hindering electrolyte accessibility and ionic transport[64]. Optimal performance was observed at a porosity of approximately 60%-70%, whereas a low porosity below 30% resulted in performance degradation due to ionic transport limitations. However, this study was conducted at a sulfur loading of approximately 4.5 mg cm^{-2} and with an excess electrolyte of 100 μL, corresponding to an E/S ratio of approximately 14.4, and thus requires further validation to assess its applicability under practical high-loading and lean electrolyte conditions.

Kim *et al.* fabricated SPAN-graphene composite electrodes via high-pressure pelletization and analyzed how electrode geometry influences electronic and ionic transport[65]. The electrode forms a densely packed two-dimensional structure of graphene nanosheets and SPAN, providing continuous electronic conduction pathways while effectively enhancing charge transport at the electrode-electrolyte interface. Low polarization and uniform reaction behavior were maintained even in this compact structure, suggesting mitigation of transport limitations under high-loading conditions. A high areal capacity of approximately 11 mAh cm^{-2} was achieved at a sulfur loading of approximately 10 mg cm^{-2}, with about 80% capacity retention after 300 cycles[65]. In addition, pouch cells demonstrated an areal capacity of approximately 6 mAh cm^{-2} with stable operation over more than 150 cycles, indicating that the structural design remains effective at the cell scale. However, SPAN-based electrodes are limited by the relatively low sulfur content of approximately 30%-45% due to sulfur being bound to the polymer backbone. Furthermore, a modified electrolyte [1 M $LiPF_6$ and 0.05 M LiDFOB in EMC:FEC (3:1 v/v)] was employed to enhance performance, making it difficult to decouple the effects of electrode structure from those of the electrolyte.

In another study, Lin *et al.* prepared hG/S composite electrodes by ball milling holey graphene (hG) with sulfur, and investigated the resulting electronic and ionic transport behavior [Figure 6A][66]. During compression, holey graphene forms a self-supporting matrix, enabling continuous electronic conduction pathways without a binder. In addition, the hole structures within the graphene sheets serve as channels for electrolyte infiltration and Li-ion transport. This is supported by the low charge-transfer resistance observed in electrochemical impedance spectroscopy (EIS). Stable electrochemical performance was reported even at a high sulfur loading of approximately 15.6 mg cm^{-2} and an E/S ratio of 6.7 μL mg^{-1}, likely due to the mitigation of ionic transport limitations typically associated with reduced porosity and increased tortuosity in dense electrodes. While electrode densification generally hinders ionic transport due to decreased porosity and increased tortuosity, the holey graphene structure in this study partially alleviates these limitations. Zuluaga-Gómez *et al.* further introduced Fe-based nanoparticles (FeNPs) into hG/S composites via dry mixing and ball milling, followed by dry pressing to form S/FeNPs/hG electrodes [Figure 6B][67]. The incorporation of FeNPs enhances electronic transport and promotes polysulfide conversion reactions, thereby improving overall reaction kinetics. A reduction in charge-transfer resistance was observed in S/FeNPs/hG electrodes compared to S/hG electrodes based on EIS analysis[67]. Stable electrochemical performance was achieved at sulfur loadings of approximately 5.72-7.01 mg cm^{-2}, demonstrating the effectiveness of introducing

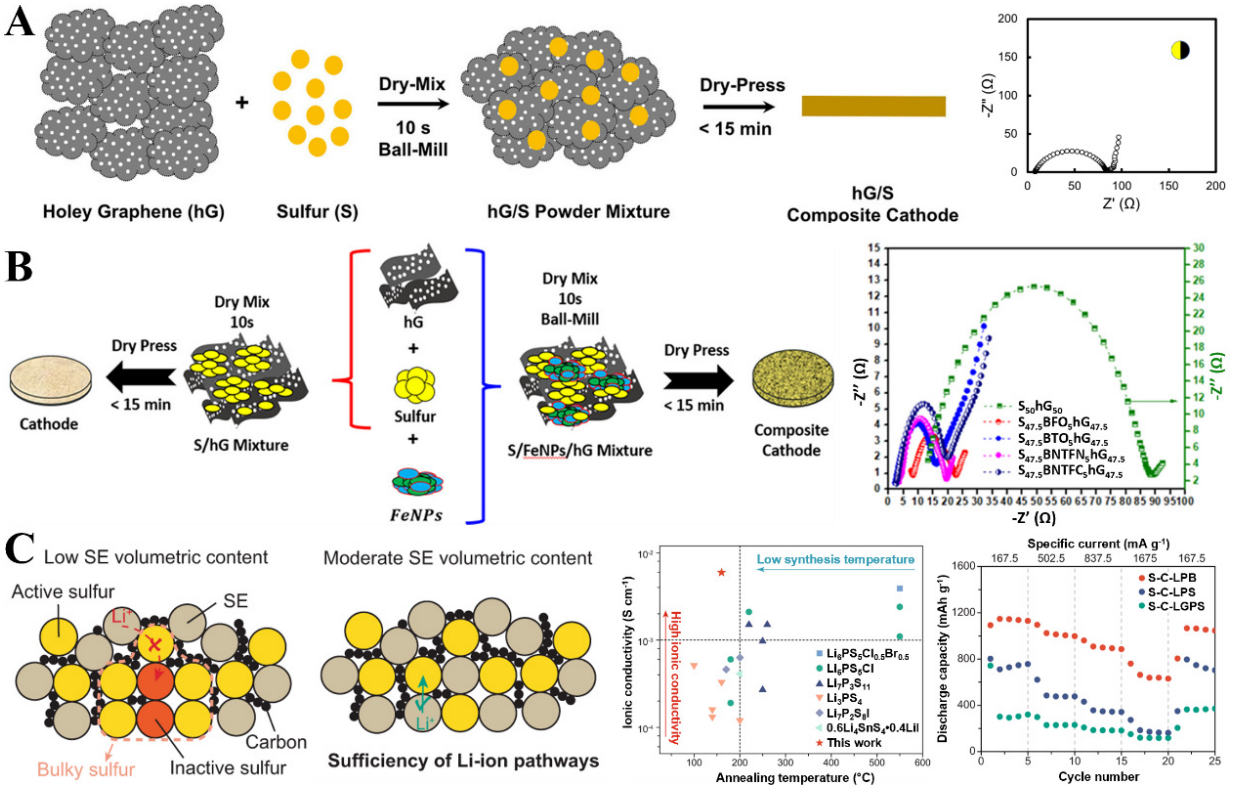

Figure 6. Representative examples of electronic and ionic transport engineering in dry electrodes fabricated via powder compression. (A) Schematic illustration of the formation process of hG/sulfur composite electrodes and corresponding EIS results. Adapted with permission from Ref.[66] Copyright © 2019 Wiley-VCH Verlag GmbH & Co. KGaA, Weinheim; (B) Schematic illustration of the structure of FeNP-incorporated hG/sulfur composite electrodes and corresponding EIS results. Reprinted from Ref.[67], under CC BY-NC-ND 4.0 license; (C) Comparison of Li-ion transport pathways and electrochemical performance as a function of SE content. Adapted from Ref.[68], under CC BY 4.0 license. SE: Solid electrolyte; LPB: Li_3PS_4-2$LiBH_4$; LPS: $Li_7P_3S_{11}$; LGPS: $Li_{10}GeP_2S_{12}$; EIS: electrochemical impedance spectroscopy; hG: holey graphene; NP: nanoparticle.

functional nanoparticles for further performance enhancement.

Wang *et al.* systematically investigated the influence of solid electrolyte (SE) volume fraction on ionic transport pathway formation in ASSLSBs [Figure 6C][68]. In this study, composite electrodes were fabricated by mixing and compressing sulfur, conductive additives, and a sulfide-based solid electrolyte, showing that Li-ion transport behavior strongly depends on the SE content[43]. At low SE content, continuous ionic pathways cannot be established, leaving a portion of sulfur electrochemically inactive and resulting in non-uniform reactions and low sulfur utilization. In contrast, when an appropriate amount of SE is introduced, the triple-phase boundary among sulfur, electrolyte, and carbon is effectively expanded, enabling continuous Li-ion pathways and improved reaction uniformity within the electrode[82]. These structural differences are reflected in electrochemical performance, where electrodes with optimized SE content exhibit high areal capacities of approximately 11 mAh cm^{-2} along with stable cycling behavior. Structural design utilizing low-density SE can effectively mitigate ionic transport limitations at solid-solid interfaces.

Overall, these studies demonstrate that various design strategies can be used to simultaneously improve electronic and ionic transport in dry-processed thick sulfur electrodes. Controlling the electronic percolation network and ionic transport pathways through the design of active materials, interfaces, and electrode structures is essential for improving electrode performance. Therefore, future research should move beyond optimizing individual components and focus on integrated electrode architecture design that enables simultaneous control of both electronic and ionic transport.

Mechanical stabilization

In dry-processed thick electrodes, mechanical stability is essential to maintain continuous electronic and ionic transport pathways during cycling. As electrode thickness and sulfur content increase, mechanical degradation such as particle detachment, interfacial delamination, and disruption of conductive networks becomes more pronounced[83]. Therefore, robust mechanical stabilization strategies are critical for achieving thick sulfur cathodes with stable electrochemical performance.

Previous studies have shown that a PTFE fibrillation-based dry process can form a three-dimensional network connecting sulfur and carbon particles[84]. Building on this concept, Sul et al. demonstrated that such a network suppresses crack formation, delamination, and contact loss in thick sulfur cathodes while improving electrode density and mechanical stability [Figure 7A][41]. In this study, wet-processed electrodes exhibited structural inhomogeneity and weak interparticle contact. In contrast, the fibrillated binder formed a continuous three-dimensional network that effectively bridges sulfur and conductive carbon, enhancing mechanical cohesion while maintaining electronic and ionic transport pathways. After 10 charge-discharge cycles, the dry-processed electrode maintains a crack-free structure compared to the wet-processed electrode. PTFE has a higher Young's modulus than the blend of poly(ethylene oxide) (PEO) and poly(vinylpyrrolidone) (PVP) binder used in slurry-based processes, resulting in reduced elastic deformation and improved mechanical stability[41]. This helps suppress crack formation within the electrode. In contrast, the PEO:PVP binder is more susceptible to deformation and is less effective in accommodating the volume changes of sulfur during cycling, leading to pulverization and contact loss[85]. As a result, the dry electrode maintains structural integrity even at high sulfur loadings of 10-12 mg cm^{-2} and delivers improved cycling stability and high areal capacities exceeding 8-10 mAh cm^{-2} compared to the wet electrode. The dry electrode also achieves a stable structure with a very low binder content of 1 wt%, enabling a higher fraction of active material and offering advantages in both electrode density and cost relative to slurry-based electrodes. This strategy is also applicable to Li_2S-based cathodes. However, the performance was demonstrated under relatively high electrolyte usage and low current rates of 1/20-1/30 C, highlighting the need for further improvements toward practical implementation.

Lv *et al.* demonstrated the mechanical stability benefits of dry thick electrodes by comparing conventional powder cathodes with sheet-type cathodes fabricated via PTFE binder fibrillation in an all-solid-state mold cell system[69]. First, a high-energy ball milling process was used to prepare a composite comprising of sulfur, $Li_7P_3S_{11}$ (LPS), and acetylene black (AB), forming an effective triphase interface for charge transport. Electrochemical performance was evaluated at an identical loading of 4.5 mg cm^{-2}. The sheet-type cathode containing PTFE exhibited slightly reduced electronic and ionic conductivities compared to the powder cathode. However, this had a limited impact on overall electrochemical performance. Rather, it improved structural stability and enabled more uniform network formation, resulting in improved performance. While little difference was observed at low current densities, the sheet-type cathode exhibited superior performance at higher current densities, likely due to its maintained mechanical stability and continuous conductive pathways during cycling[86]. Furthermore, a sheet-type LiSiPSCl solid electrolyte was fabricated using a similar process and assembled into a full cell with a lithiated silicon anode. The resulting cell delivered an initial capacity of 1,512.2 mAh g^{-1} at a high current density of 1 mA cm^{-2} (0.2 C) and retained 1,067.4 mAh g^{-1} after 30 cycles. Despite these results, the study employed a relatively low sulfur content of about 40 wt%, indicating that further improvements are required to achieve high-energy density.

Overall, these studies demonstrate that mechanical stability in dry thick sulfur electrodes is not merely a structural factor, but a key parameter governing continuous charge transport and overall electrode performance. Fibrillated binder networks are effective for improving interparticle cohesion and maintaining stable conductive pathways. However, challenges remain in simultaneously achieving high sulfur loading,

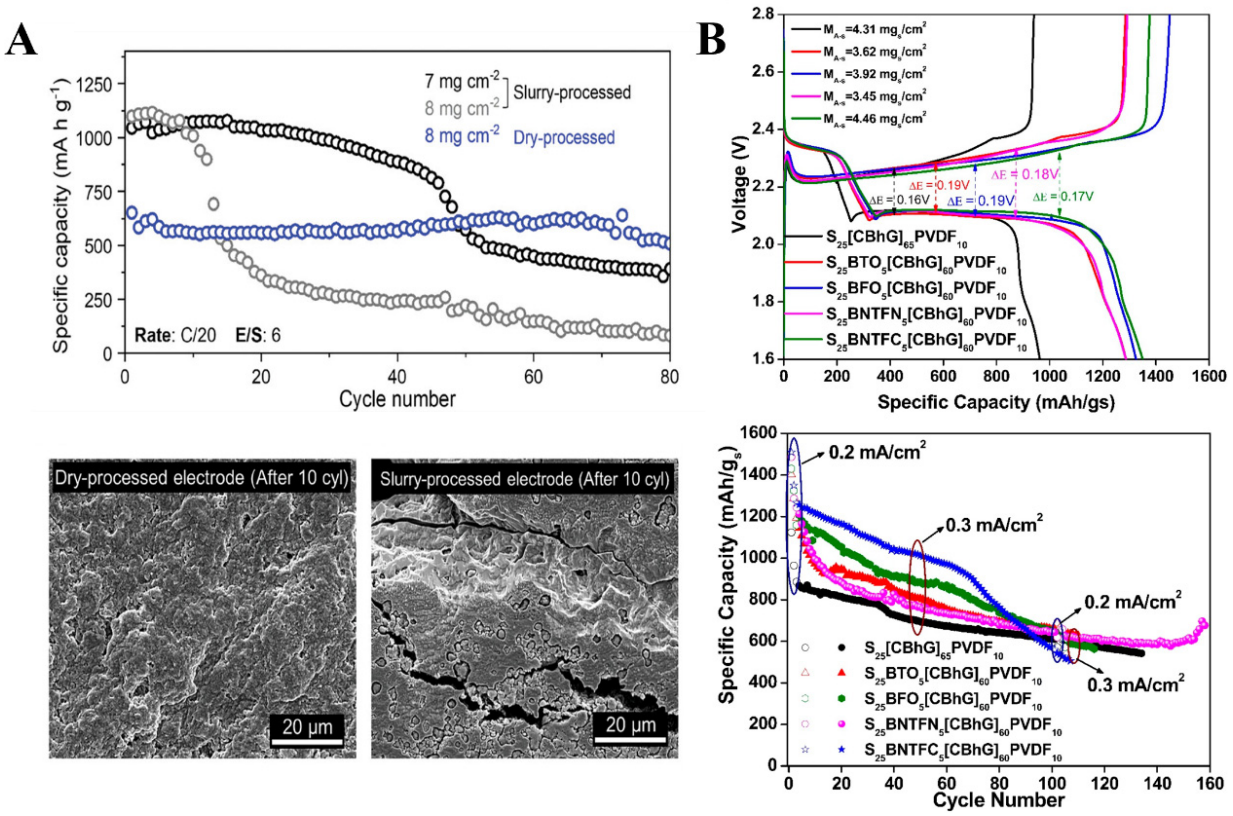

Figure 7. (A) Cycling performance of high-loading sulfur electrodes fabricated via wet and dry processes, and SEM images of electrode surfaces after 10 cycles. Reprinted with permission from Ref.[41] Copyright © 2024 Wiley-VCH GmbH; (B) Electrochemical performance comparison of electrodes incorporating FNPs into hG structures for polysulfide shuttle suppression. Reprinted from Ref.[72], under CC BY 4.0 license. hG: Holey graphene; PVDF: poly(vinylidene fluoride); SEM: scanning electron microscopy; FNP: ferroelectric nanoparticle.

low electrolyte consumption, and practical operating conditions. Therefore, future research should focus on precisely controlling the relationships between binder fibrillation behavior, interparticle contact, and electrode architecture to achieve both mechanical stability and efficient charge transport.

Shuttle suppression

In thick LSB electrodes, targeting high-energy-density, low E/S conditions can exacerbate local concentration gradients, reaction heterogeneity, and non-uniform polysulfide conversion within the electrode. As a result, LiPSs may accumulate in specific regions and diffuse out of the cathode, leading to severe shuttle effects, reduced sulfur utilization, and accelerated capacity fading[56]. Therefore, thick sulfur electrodes require shuttle suppression strategies beyond simple physical confinement. Functional hosts and additives should be designed to effectively enhance polysulfide adsorption, suppress their migration, and promote uniform redox reactions throughout the electrode.

Chen *et al.* effectively suppressed the polysulfide shuttle in dry thick sulfur electrodes by employing vanadium nitride quantum dots (VNQDs) incorporated into N, O, S co-doped hierarchical porous carbon (NOSHPC)[70]. The NOSHPC host was synthesized via thermal treatment of acesulfame potassium, followed by the incorporation of highly dispersed VNQDs using ammonium vanadate and hexamethylenetetramine. The polar nature and catalytic properties of VN enable strong chemical adsorption of LiPSs and accelerated redox conversion, thereby promoting more uniform reactions even under high-loading conditions[87,88]. In addition, the hierarchical porous structure maintains effective ionic and electronic transport pathways, thereby alleviating transport limitations in thick electrodes. As a result, the electrode exhibited a high initial

capacity of 1,655 mAh g^{-1} at 0.1 C and excellent long-term stability, with a very low capacity decay rate of 0.0107% per cycle over 1,000 cycles at 1 C. Together with high coulombic efficiency, these results indicate effective suppression of the polysulfide shuttle. Furthermore, at the pouch-cell level, the sulfur loading was extended from 5.2 to 18.6 mg cm^{-2}, achieving an areal capacity of 14.2 mAh cm^{-2} and an energy density of 462 Wh kg^{-1} at an E/S ratio of 5.3. These results are close to practical high-energy-density levels. However, limitations remain in process complexity and material synthesis costs, and further optimization is required to maintain performance under more stringent lean electrolyte conditions.

Dörfler *et al.* elucidated the polysulfide reaction mechanism in nitrogen-doped carbon-based sulfur cathodes and proposed fundamental design principles for shuttle suppression[71]. Nitrogen-doped carbon interacts chemically with LiPSs, enabling not only physical confinement but also simultaneous regulation of polysulfide adsorption and redox kinetics. This behavior plays a key role in suppressing polysulfide dissolution and improving reaction reversibility, even under reduced electrolyte conditions. In this study, a template-assisted porous structure was combined with N-doped carbon to precisely control interactions with LiPSs, and the nitrogen content was optimized to identify favorable conditions[71]. The sulfur loading was increased to approximately 4 mg cm^{-2}, and stable cycling with high capacity retention was achieved under relatively low E/S ratios. These findings provide an important basis for designing high-loading, lean-electrolyte LSB systems. However, the sulfur loading remains moderate, and the absence of pouch-cell validation indicates that further verification is required for practical applications.

Zuluaga-Gómez *et al.* proposed an alternative approach for suppressing the polysulfide shuttle by incorporating ferroelectric nanoparticles (FNPs) into a hG structure [Figure 7B][72]. In this system, the hG framework provides a porous structure that facilitates ion and electron transport while accommodating high sulfur loading. The introduced ferroelectric nanoparticles electrostatically adsorb and immobilize polysulfides via internal polarization. This polarization-induced chemical confinement is more effective than simple physical trapping and contributes to improved reversibility of redox reactions. Upon incorporation of ferroelectric materials, the electrode exhibited improved capacity and cycling stability, consistent with previous studies reporting that ferroelectric additives can enhance electrochemical performance in LSB systems[89]. These findings suggest that, in dry thick electrode systems, shuttle suppression requires not only structural design but also the incorporation of electrostatic and polarization-driven chemical interactions. Despite the improved performance, the study was conducted at a relatively high E/S ratio of approximately 7, and the sulfur fraction remained low at approximately 25 wt%, which limits its applicability to practical high-energy-density conditions. This suggests that further optimization is necessary for application at the pouch-cell level.

Overall, shuttle suppression in dry thick sulfur electrodes has evolved beyond physical confinement toward actively controlling polysulfide behavior. Approaches involving polar surfaces, catalytic active sites, heteroatom doping, and polarization-driven interactions enable simultaneous regulation of LiPS adsorption and conversion reactions, contributing to more uniform and reversible electrochemical behavior even under low E/S conditions. However, most studies still rely on limited sulfur loading, relatively high electrolyte consumption, or complex material designs, which limit their applicability in terms of practical energy density and process scalability. Therefore, future research should focus on developing functional host materials with simplified and cost-effective synthesis, as well as electrode architecture strategies that can simultaneously achieve high loading and low E/S conditions.

EXAMPLES OF DRY THICK ELECTRODES IN OTHER SYSTEMS AND APPLICABILITY TO LSB

In LIB systems, various strategies have been proposed to control the structure of dry thick electrodes while improving charge transport and mechanical stability[90]. These approaches encompass electrode architecture design as well as multifunctional binders, additives, and optimized processing conditions. However, their

direct application to LSB systems remains limited because sulfur-based electrodes face more severe challenges, including low electrical conductivity, polysulfide migration, and strong reaction heterogeneity in thick electrodes. Therefore, these strategies should be tailored to the specific characteristics of LSB systems rather than directly transferred. This section reviews recently reported dry thick-electrode design strategies in LIBs and discusses their applicability to LSB systems.

Additive manufacturing-based 3D printing has emerged as a processing approach that enables precise control of electrode architecture, where materials are deposited layer by layer to form structured electrodes. In this strategy, infill geometry can be tuned to control internal porosity and electrolyte infiltration characteristics. Some studies have proposed solvent-free 3D printing of dry electrodes using thermoplastic extrusion-based melt processing. For example, Park *et al.* proposed a structured electrode additive manufacturing (SEAM) process, in which a feedstock composed of graphite flake as the active material, carbon additives, and a thermoplastic polymer is extruded in a molten state [Figure 8A][91]. In this process, the polymer is melted by heat, and shear flow aligns the feedstock along the printing direction, resulting in a structure with low tortuosity along the electrode thickness. The printed electrode subsequently undergoes debinding and sintering at high temperatures of 400-600 °C, removing the polymer and converting the structure into a free-standing carbonaceous electrode. Such architecture can shorten Li-ion transport pathways, enabling improved transport properties and electrochemical performance even in millimeter-thick graphite electrodes.

However, the direct application of such high-temperature processes to LSB systems requires careful consideration of sulfur's intrinsic properties. Sulfur exhibits significant evaporation above 150-200 °C and readily vaporizes at temperatures above 400 °C, leading to substantial sulfur loss. Therefore, for LSBs, strategies that retain functional polymers within the electrode, rather than removing them, may be more suitable. In this context, Maurel *et al.* reported an approach in which a filament was prepared by mixing an active composite of lithium terephthalate (Li_2TP) and carbon black with a polylactic acid (PLA) polymer matrix, followed by direct printing of the electrode via fused deposition modeling (FDM) [Figure 8B][92]. In this method, the polymer is not removed but remains within the electrode to maintain structural integrity, and the process is carried out at relatively low temperatures of 170-180 °C. While this approach can mitigate complete sulfur loss, the processing temperature remains sufficiently high to limit direct application to sulfur-based cathodes. In addition, molten sulfur exhibits low viscosity, which can lead to redistribution within the electrode and difficulty in maintaining structural uniformity. These studies suggest potential routes for extending 3D printing strategies to LSB systems through materials design. For example, the use of low-temperature processable polymers compatible with the thermal stability range of sulfur, as well as sulfurized polymers or immobilization strategies that suppress sulfur migration and volatilization, may offer viable routes to adapt additive manufacturing approaches to LSB electrodes.

In binder fibrillation-based dry electrode processes, PTFE is widely used as a representative binder that simultaneously satisfies high-voltage stability and fibrillation capability. A strategy has been proposed to enhance adhesion between active materials and PTFE by designing the active material structure. Kang *et al.* introduced polymeric species such as poly(acrylic acid)-grafted sodium carboxymethyl cellulose (PC) onto the surface of lithium nickel cobalt manganese oxide (NCM) cathode particles to create bollard sites that effectively anchor PTFE[93]. These sites strengthen interfacial bonding between the active material and PTFE, thereby improving mechanical stability and stabilizing the conductive network. This concept can be extended to LSB systems. For example, introducing similar bollard sites on the surface of spherical carbon particles that host sulfur, or on carbon nanotube (CNT)-based conductive networks, could enhance adhesion with PTFE. However, in LSBs, the design of such sites must also consider interactions with LiPS. If the introduced structures interact too strongly with LiPS, they may restrict mass transport or alter reaction

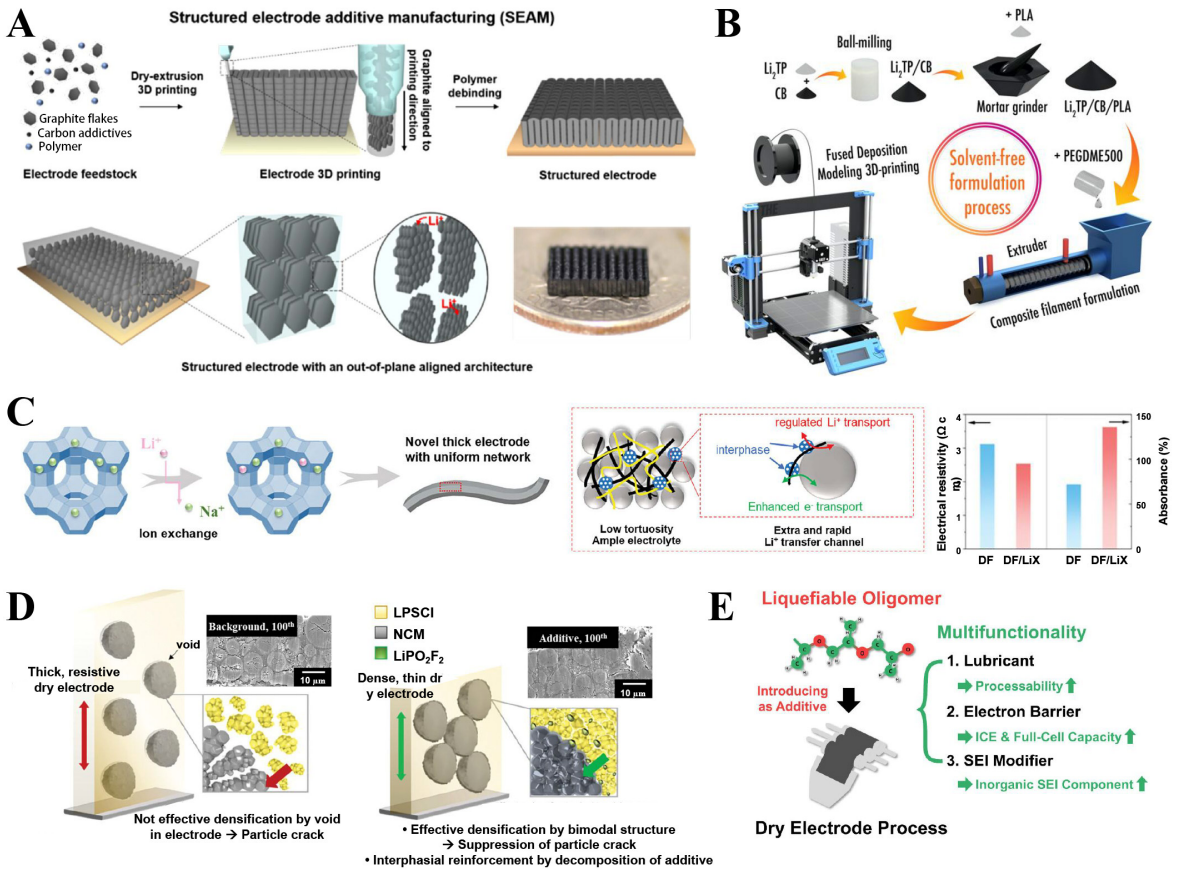

Figure 8. Various processing and material design strategies for dry thick electrode design. (A) Formation of 3D-printed electrodes via SEAM and development of through-thickness aligned structures. Reprinted with permission from Ref.[91] Copyright © 2022, American Chemical Society; (B) Schematic illustration of electrode fabrication using FDM. Reprinted from Ref.[92], under CC BY 4.0 license; (C) Expansion of Li-ion transport pathways and formation of low-tortuosity structures via Li-X zeolite incorporation. Adapted with permission from Ref.[94] Copyright © 2024 Wiley-VCH GmbH; (D) Electrode densification and interfacial stabilization via $LiPO_2F_2$ additive incorporation. Adapted with permission from Ref.[99] Copyright © 2023 Wiley-VCH GmbH; (E) Surface coating and multifunctional enhancement using liquefiable oligomer-based PPG additives in the dry process. Reprinted with permission from Ref.[100] Copyright © 2026, American Chemical Society. TP: Terephthalate; CB: carbon black; PLA: polylactic acid; PEGDME: poly(ethylene glycol) dimethyl ether; DF: dry film; LPSCl: lithium phosphorus sulfur chloride; NCM: lithium nickel cobalt manganese oxide; SEAM: structured electrode additive manufacturing; FDM: fused deposition modeling; PPG: poly(propylene glycol).

locations. Therefore, designing bollard materials that interact effectively with LiPS to immobilize them may improve reaction uniformity and structural stability while also contributing to shuttle suppression in dry, thick LSB electrodes.

In addition, LIB research has actively explored multifunctional additives that simultaneously regulate electronic and ionic transport as well as interfacial properties. For instance, studies employing lithium-ion-exchanged zeolite (Li-X zeolite) as an additive have reported improved transport properties in ultrahigh-loading dry thick electrodes by jointly controlling porosity and tortuosity, thereby facilitating Li-ion transport [Figure 8C][94]. Furthermore, the formation of a stable cathode-electrolyte interphase suppresses side reactions. However, when applied to LSB systems, additional considerations regarding sulfur reactivity and polysulfide accommodation are required. Pristine zeolites before Li-ion exchange may exhibit Brønsted or Lewis acidity, which can induce side reactions with polysulfide species or lead to irreversible sulfur loss[95,96]. Li-exchanged zeolites may mitigate this acidity, but direct verification is still required. Given that solvated LiPSs have a size of approximately 1.5 nm, the micro- and mesopores of Li-X zeolites ranging from 1-6 nm can contribute to shuttle suppression via physical confinement[97]. However, excessive adsorption or

restricted diffusion within pores may hinder reversible sulfur conversion and induce reaction inhomogeneity, particularly in thick electrodes. Therefore, in designing zeolite-based additives for thick LSB electrodes, it is essential to balance additive-sulfur interactions against the trade-off between polysulfide confinement and transport.

Beyond porous additives, one-dimensional (1D) conductive additives have attracted attention as multifunctional components for reinforcing electronic percolation networks within dry-processed electrodes. For example, the incorporation of carbon fibers into dry thick NCM811 electrodes has been shown to improve electronic transport by forming more effective conductive pathways[98]. In particular, 1D carbon fibers can establish percolation networks along the electrode thickness, thereby maintaining electrical connectivity even in thick electrodes. However, when applied to LSB systems, although carbon fibers enhance electronic conductivity, their relatively weak interaction with polysulfides limits their ability to suppress the shuttle effect. Therefore, to utilize carbon fibers in dry thick LSB electrodes, surface modification or hybridization with additional functional materials that can regulate polysulfide interactions should be further developed.

Interphase-forming additives for stabilizing the electrode-electrolyte interface play an important role in dry thick electrode design. For instance, the introduction of $LiPO_2F_2$ as an additive has been shown to fill interparticle voids, induce electrode densification, and suppress particle cracking through more uniform pressure distribution in dry thick electrodes [Figure 8D][99]. As a result, both ionic and electronic conductivities are improved, resulting in more stable transport characteristics even in thick electrodes. In addition, $LiPO_2F_2$ decomposes during initial cycling to form LiF- and Li_xPF_y-based interfacial layers, which suppress side reactions and enhance interfacial stability. However, for sulfur electrodes, such decomposition-derived interphases may interact with polysulfides, thereby altering interfacial composition. In particular, LiF-rich layers may act as barriers that suppress polysulfide migration while increasing ionic transport resistance. Therefore, applying such interphase-forming additives to LSB systems requires careful design that balances polysulfide reactivity and transport with interfacial stability.

More recently, multifunctional additives compatible with dry processing have been proposed. For example, poly(propylene glycol) (PPG), a liquefiable oligomer, has been introduced as a liquefiable additive that softens at 80 °C during dry electrode processing, enabling uniform coating of particle surfaces without the use of solvents [Figure 8E][100]. This approach effectively overcomes dispersion limitations associated with conventional dry processes. PPG can simultaneously act as a lubricant to promote PTFE fibrillation, as a barrier that suppresses electron transport and prevents binder decomposition, and as a modifier of Li-ion solvation structure that promotes the formation of inorganic-rich SEI. When applied to LSB systems, the relatively mild processing temperature avoids significant sulfur volatilization or structural transformations, such as ring opening or polymerization, thereby providing processing advantages[101,102]. However, in LSBs, oligomer coatings may interact with polysulfides. In addition, while organic additives such as PPG may facilitate Li-ion transport, they can also hinder electron transport, potentially slowing sulfur conversion kinetics. Therefore, the application of such additives to thick LSB electrodes requires careful design that considers interactions with polysulfides, reaction distribution, and charge transport.

Overall, dry thick electrode design strategies developed for LIB systems have evolved toward integrated approaches that jointly optimize electronic and ionic transport, interfacial reactions, and structural stability through process control, binder compatibility, and multifunctional additives. However, in LSB systems, severe reaction heterogeneity and interfacial instability caused by polysulfide migration require system-specific redesign rather than the direct adoption of LIB strategies. For example, process-based structural control should consider the thermal stability and spatial distribution of sulfur, while binder and additive

design should simultaneously address polysulfide interactions, balanced ion/electron transport, and interfacial reaction control.

ADVANCED CHARACTERIZATION OF DRY-PROCESSED THICK SULFUR CATHODES

LSBs are characterized by complex reaction mechanisms involving multistep sulfur conversion reactions and the formation and migration of various polysulfide species during cycling. In dry process-based thick sulfur cathodes, microstructural features such as interparticle contact, pore networks, and binder fibrillation structures significantly influence electrochemical reaction behavior. In addition, sulfur dissolution and precipitation, as well as structural evolution of the electrode during cycling, are closely linked to performance degradation[56]. To accurately understand these processes, *operando* and *in situ* electrochemical analysis techniques are required to track reaction behavior during cell operation, along with microstructural characterization methods to precisely probe internal electrode structure. This section first introduces *operando* and *in situ* electrochemical techniques for analyzing reaction behavior, followed by microstructural characterization methods for investigating the structural features of dry thick sulfur cathodes.

Operando and *in situ* electrochemical analysis

Operando Raman spectroscopy enables real-time observation of changes in chemical bonding and the formation and consumption of reaction intermediates within electrodes during battery operation. In LSB systems, *operando* Raman analysis can track the chemical state evolution of various species such as sulfur, LiPSs, and Li_2S, allowing direct observation of the formation and disappearance of individual polysulfide species during conversion reactions. It is therefore widely used to elucidate reaction mechanisms. In thick sulfur electrodes, interpretation of the formation pathways and reaction mechanisms of intermediates is critical for understanding the system, making *operando* Raman an effective analytical tool. For example, Kim *et al.* reported the reaction mechanism and reversibility of thick sulfur cathodes with a sulfur loading above 5 mg cm^{-2} using *operando* Raman analysis[65]. As discharge proceeded, the intensity of S-S and C-S bond peaks originating from SPAN gradually decreased and eventually disappeared at the end of discharge. During the subsequent charge process, these peaks reappeared, indicating that S-S bonds are reversibly broken during discharge and reformed upon charging. These results demonstrate the reversible lithium storage capability of SPAN-based thick cathodes and highlight the usefulness of *operando* Raman in elucidating LSB reaction mechanisms. However, this technique has potential limitations in interpretation for thick electrodes. Volume changes during cycling can shift the Raman beam focal plane, complicating quantitative analysis of real-time signals. In addition, dissolution and migration of polysulfide species may alter the distribution of active species within the probed region over time. Furthermore, because reactions proceed non-uniformly along the electrode thickness in thick electrodes, Raman signals reflect localized rather than bulk reaction behavior. Therefore, *operando* Raman results for thick electrodes should be interpreted with consideration of such spatial and dynamic inhomogeneities. In this regard, approaches such as confocal Raman analysis, which provides depth-resolved information, or the design of directional probes to control laser incidence, may help resolve spatial inhomogeneity.

Operando X-ray diffraction (XRD) enables real-time tracking of crystal structure changes during cycling and provides critical insight into phase evolution in LSB conversion reactions. It enables quantitative evaluation of reaction kinetics and conversion efficiency, making it useful for assessing the kinetics of sulfur formation and decomposition and the reaction mechanisms in thick electrodes. It can also be employed to identify incomplete conversion or residual sulfur in thick electrodes. For instance, Dörfler *et al.* investigated phase evolution and Li_2S formation behavior during cycling in thick sulfur electrodes using nitrogen-doped porous carbon as a sulfur host[71]. During discharge, a decrease in sulfur peaks accompanied by the formation of Li_2S crystalline phases was observed, reflecting the reduction of sulfur to Li_2S. In undoped carbon, Li_2S peaks appeared at approximately 85% depth of discharge (DOD). This observation is consistent with previous

in situ X-ray absorption near-edge structure studies reported by the Nazar group[103]. In contrast, Li_2S nucleation in N-doped carbon was observed at around 50% DOD, indicating improved nucleation kinetics. In both cases, Li_2S growth followed an exponential trend, suggesting a similar growth mechanism, with the primary difference arising from the nucleation stage. These results demonstrate that *operando* XRD can provide insight into Li_2S nucleation and reaction mechanisms in thick sulfur cathodes. However, since *operando* XRD provides bulk-averaged signals, it is difficult to directly resolve local reaction heterogeneity in thick electrodes where reactions proceed non-uniformly. In particular, spatial variations within the electrode may not be fully captured, and such limitations should be considered when interpreting the results. To address this, two approaches can be used: controlling X-ray penetration depth to selectively probe specific regions, and analyzing temporal differences in phase evolution to infer spatial heterogeneity. In thick electrodes, where reactions proceed sequentially rather than uniformly across the electrode thickness, phase transitions observed in *operando* XRD appear temporally broadened. Such temporal broadening can serve as an indirect indicator of spatial inhomogeneity in the electrode's reaction.

In situ EIS is a powerful technique for probing charge transfer characteristics and reaction kinetics at the electrode-electrolyte interface during battery operation. In LSB systems, the formation of various intermediates during sulfur conversion reactions alters charge-transfer resistance at the interface. Therefore, *in situ* EIS enables tracking of reaction kinetics and interfacial evolution during operation. For example, Cronk *et al.* performed *in situ* EIS measurements at different states of charge after formation cycles to evaluate the reversibility of thick sulfur cathodes in ASSLSBs [Figure 9A][62]. In the discharged state at 1 V, the formation of Li_2S increased the charge transfer resistance, resulting in an enlarged semicircle in the Nyquist plot and an overall increase in impedance. In contrast, in the charged state at 3 V, Li_2S oxidation reduced the charge transfer resistance, and the impedance approached that of the open-circuit voltage (OCV) state. These results indicate that charge transfer resistance at the electrode-electrolyte interface changes reversibly with Li_2S formation and oxidation. However, such interpretations are often based on specific material systems, and EIS analysis for thick electrodes requires a broader perspective. As electrode thickness, sulfur loading, or electrode density increases, changes in pore structure, including increased tortuosity and reduced electrolyte accessibility, can significantly increase ionic transport resistance[104]. These effects are reflected in changes in the low-frequency diffusion resistance region of the Nyquist plot or in overall impedance increases. Therefore, for thick electrodes, EIS should be interpreted beyond simple changes in charge-transfer resistance (R_{ct}) through systematic comparison of impedance behavior as a function of structural parameters such as electrode thickness, sulfur loading, and density. This approach enables more precise separation of interfacial reactions from internal transport limitations. For example, comparing EIS results of electrodes with different sulfur loadings can help distinguish whether performance degradation is dominated by interfacial reactions or by internal ionic transport limitations[105,106], based on changes in high-frequency semicircles and low-frequency diffusion features. Similarly, analysis of impedance variations with electrode density can provide insight into how densification-induced pore structure changes affect ion transport pathways and reaction distribution.

From this perspective, EIS can reflect not only transport limitations but also changes in electrical connectivity arising from structural evolution within the electrode. For example, Kim et al. compared impedance evolution during cycling between wet-processed (S/Se-SPAN) and dry-processed (D/Se-SPAN) selenium-doped SPAN cathodes [Figure 9B][63]. In wet electrodes, a new semicircle (R_{int}) appeared and increased continuously in the low-frequency region during cycling, which can be interpreted as degradation of the electrical contact and deterioration of the percolation network. In contrast, the mechanically robust conductive network formed by multi-walled carbon nanotubes (MWCNTs) and fibrillated PTFE in dry electrodes can effectively maintain electrical connectivity and suppress interfacial resistance increase, as similarly reported in previous dry electrode studies[86]. The suppressed growth of R_{ct} and R_{int} indicates that a

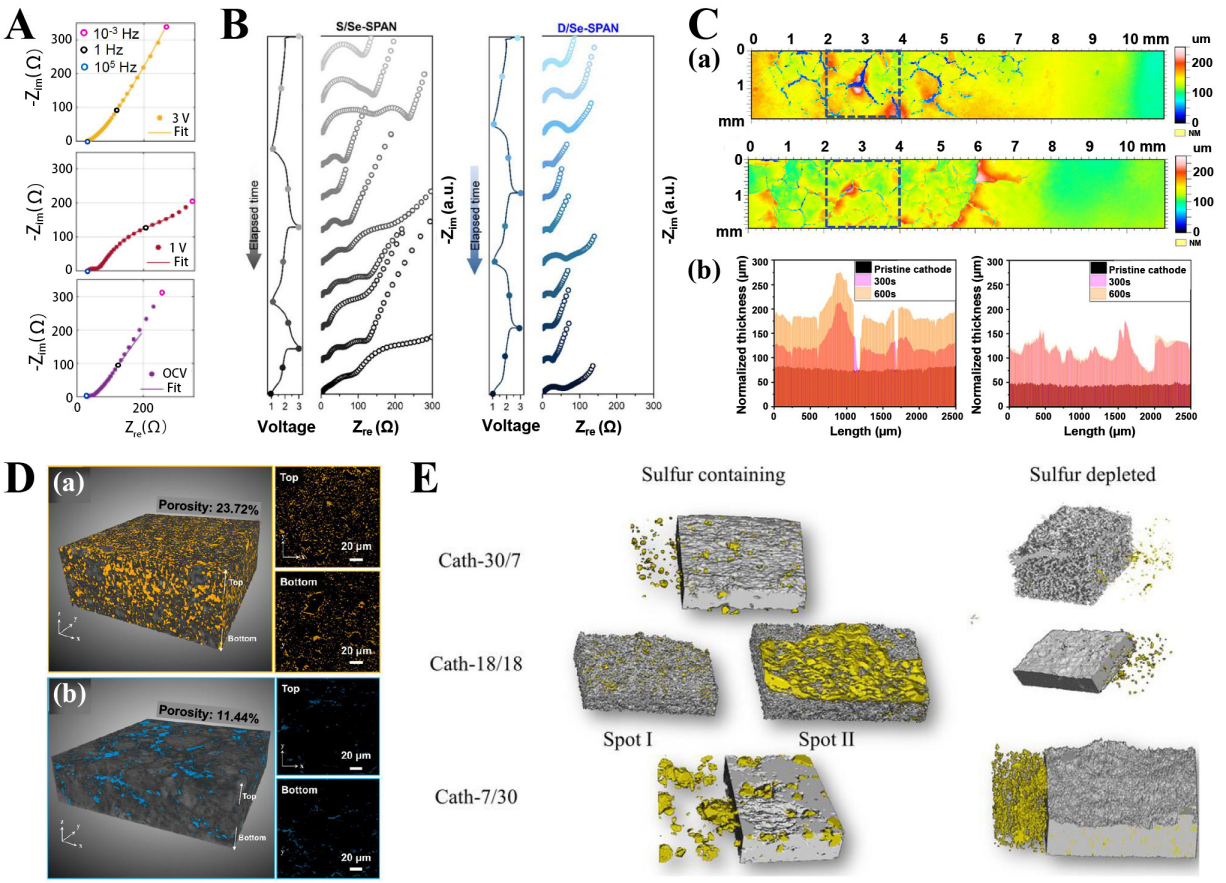

Figure 9. (A) *In situ* EIS Nyquist plots of ASSLSBs with dry sulfur electrodes measured at different states of charge (OCV, 1 V discharge, and 3 V charge). Reprinted from Ref.[62], under CC BY 4.0 license; (B) Comparison of EIS evolution during initial cycles in SPAN-based lithium-sulfur batteries for wet-processed S/Se-SPAN (left) and dry-processed D/Se-SPAN (right). Reprinted from Ref.[63], under CC BY 4.0 license; (C) Confocal microscopy analysis of surface and thickness changes in dry sulfur cathodes after electrolyte infiltration: (a) extended surface topography maps of uncompressed (top) and compressed (bottom) electrodes, and (b) extracted height profiles after electrolyte infiltration for uncompressed (left) and compressed (right) electrodes. Reprinted from Ref.[107], under CC BY 4.0 license; (D) Internal structures of (a) wet-processed S/Se-SPAN electrodes and (b) dry-processed D/Se-SPAN electrodes, compared using 3D X-ray microscopy-based μCT. The carbon matrix is shown in gray, and sulfur is shown in orange and blue, respectively. Reprinted from Ref.[63], under CC BY 4.0 license; (E) Three-dimensional structure of a dry-processed S/C cathode reconstructed by synchrotron X-ray tomography. The carbon matrix is shown in gray, and sulfur is shown in yellow. Reprinted from Ref.[108], under CC BY 4.0 license. SPAN: Sulfurized polyacrylonitrile; EIS: electrochemical impedance spectroscopy; ASSLSB: all-solid-state lithium-sulfur battery; μCT: micro-computed tomography.

stable electrode structure helps maintain charge transfer kinetics during cycling. These results demonstrate that EIS serves as a multidimensional analytical tool capable of probing not only interfacial reactions but also internal transport properties and structural stability. This is particularly important for thick electrodes, where interactions among structure, transport, and interfacial phenomena critically determine performance.

Overall, *operando* Raman, *operando* XRD, and *in situ* EIS analyses provide complementary insights into chemical bonding changes, phase transitions, and charge transfer behavior at the electrode-electrolyte interface, enabling a comprehensive understanding of LSB conversion mechanisms. While these techniques allow real-time or state-specific tracking of electrochemical reactions, they have limitations in directly resolving microstructural changes, such as internal electrode structure or spatial distribution of sulfur species, which are particularly important in dry thick electrodes. Therefore, a combined approach incorporating microstructural analysis is required to achieve a more comprehensive understanding of electrode structure and sulfur distribution in dry thick cathodes.

Microstructural analysis

To understand microstructural characteristics governing the performance of dry thick sulfur electrodes, various microstructural characterization techniques have been employed. In this section, ex situ confocal microscopy, 3D X-ray-based tomography, and small-angle X-ray scattering (SAXS) are introduced as representative techniques for analyzing the structural features of dry thick sulfur cathodes. Ex situ confocal microscopy enables observation of the three-dimensional morphology and thickness variation of electrode surfaces and is particularly useful for visualizing wetting and swelling behavior during electrolyte infiltration. By reconstructing height distributions from multiple two-dimensional images acquired at different depths, electrode thickness changes and surface deformation can be quantitatively evaluated. Schmidt *et al.* investigated the time-dependent swelling behavior of dry-processed sulfur electrodes upon electrolyte wetting using confocal microscopy, comparing compressed and uncompressed electrodes[107]. In uncompressed electrodes, electrolyte contact led to significant swelling as the electrolyte penetrated into the electrode, resulting in a marked increase in thickness and rapid changes in surface morphology [Figure 9C(a)]. Within the wetted region, thickness increased by several hundred micrometers, accompanied by the formation of cracks and fissures extending over several thousand micrometers. This behavior is attributed to the buildup of internal mechanical stress during electrolyte infiltration, which is partially released through delamination of the active material layer. In addition, crack formation is likely associated with insufficient cohesion among electrode components due to the relatively weak binding strength of the PTFE binder. In contrast, compressed electrodes exhibited smaller cracks and less thickness variation[107]. In some regions, wrinkle-like structures were observed near the edges of the wetted area, arising from lateral expansion of the electrode. Quantitative analysis of thickness evolution based on height profiles extracted from a smaller region (2,500 × 2,500 μm^2) further confirms the time-dependent swelling behavior following electrolyte infiltration [Figure 9C(b)]. For uncompressed electrodes, the thickness increased from approximately 80 μm to 120 μm at 300 s after electrolyte contact, then to 180 μm at 600 s. In contrast, the compressed electrodes increased from approximately 47 μm to 120 μm after approximately 600 s. The more rapid expansion observed in compressed electrodes is attributed to the release of accumulated mechanical stress during electrolyte infiltration. These findings suggest that the initial electrode density established by dry processing may change significantly after electrolyte infiltration and may not be maintained during battery operation. Consequently, comparisons of cell performance based solely on initial electrode density may be limited. Overall, this study highlights that confocal microscopy is a useful technique for simultaneously capturing surface morphology and thickness evolution in electrodes.

3D X-ray-based tomography is a widely used non-destructive technique for reconstructing and characterizing the internal microstructure of electrodes in three dimensions. By exploiting differences in X-ray absorption, it enables visualization of pore structures, particle distribution, and structural uniformity along the electrode thickness. It is particularly useful for thick or high-loading electrodes, where pore distribution and structural uniformity strongly affect ion transport and reaction homogeneity. For example, Kim et al. performed micro-computed tomography (μCT) analysis using 3D X-ray microscopy to investigate the internal structure of Se-SPAN-based sulfur cathodes fabricated via a dry process[63]. Comparison of reconstructed 3D images of wet-processed (S/Se-SPAN) and dry-processed (D/Se-SPAN) electrodes reveals that wet electrodes exhibit a relatively high porosity of approximately 23.72% along with structural inhomogeneity and numerous voids across the electrode thickness [Figure 9D(a)]. These features arise from binder migration in the presence of solvent and void formation during solvent evaporation. In contrast, dry-processed electrodes display a lower porosity of approximately 11.44% and a more compact structure [Figure 9D(b)]. These results indicate that dry processing enables the formation of dense electrodes, which can enhance electrical connectivity and structural stability while also reducing electrolyte uptake, thereby facilitating lower electrolyte-to-active material ratios. However, μCT has limited resolution for resolving sulfur distribution due to the low contrast in X-ray absorption between sulfur and the carbon matrix.

To overcome this limitation, synchrotron X-ray tomography has been introduced. Synchrotron-based techniques offer higher brightness and spatial resolution, enabling detailed analysis of sulfur distribution, carbon matrix structure, and interparticle pore networks. Schmidt et al. used synchrotron X-ray tomography to analyze the internal structure of sulfur/carbon composite cathodes prepared via a dry process and demonstrated that sulfur distribution strongly depends on the composition of conductive additives [Figure 9E][108]. Here, Cath-A/B denotes the relative composition of conductive additives, where A and B correspond to ketjen black (KB) and MWCNTs, respectively. In KB-rich Cath-30/7, sulfur shows a relatively uniform distribution within the carbon matrix, whereas in Cath-18/18, sulfur tends to accumulate near the separator-facing cathode surface. In Cath-7/30, which contains a higher fraction of MWCNTs, large sulfur agglomerates are observed within the carbon matrix, indicating that sulfur is predominantly stored in macropores. These results demonstrate that the structural characteristics of the carbon matrix directly govern the location and distribution of sulfur. Furthermore, an increase in total porosity after thermal removal of sulfur indirectly suggests that sulfur had originally occupied pores in the carbon matrix. For quantitative analysis of pore size distribution and porosity, complementary techniques such as mercury intrusion porosimetry can be employed to further elucidate the relationship between sulfur storage behavior and pore structure in dry-processed electrodes.

Beyond *ex situ* structural analysis, *in situ* tomography techniques have recently attracted attention for real-time tracking of structural evolution within electrodes. For example, *in situ* nano X-ray tomography studies on LIB pouch cells have revealed three-dimensional structural evolution and reaction distribution during charging, demonstrating that crack formation induced by volume expansion can limit ion transport pathways and lead to reaction inhomogeneity[109]. These findings highlight that *in situ* tomography serves as a powerful tool for directly probing the interplay among structure, transport, and interfacial phenomena within electrodes. Therefore, applying *in situ* tomography to dry thick sulfur electrodes is expected to play a key role in elucidating sulfur reactivity, transport behavior, and reaction non-uniformity along the electrode thickness.

Furthermore, SAXS can be utilized to analyze nanoscale pore structures and pore size distributions within electrodes. SAXS has been applied in non-thick LSB systems to investigate pore size distributions within carbon hosts, sulfur storage behavior, and pore filling characteristics[110-112]. In thick sulfur electrodes, where electrolyte infiltration and ion transport may be limited, only a fraction of internal pores may participate in reactions. Therefore, SAXS can indirectly estimate pore utilization by analyzing pore filling behavior. For example, when comparing chord-length distribution profiles at different DOD, selective changes in peak intensities within specific pore size domains, rather than uniform changes across all domains, can indicate reaction inhomogeneity[110]. Conversely, uniform changes across multiple pore domains suggest more homogeneous reaction behavior. Thus, SAXS can serve as a complementary technique for evaluating pore structure, sulfur storage behavior, and structural evolution in thick sulfur electrodes.

Overall, microstructural characterization techniques, including ex situ confocal microscopy, 3D X-ray tomography, synchrotron X-ray tomography, and SAXS, serve as powerful tools for analyzing thick electrodes. These approaches provide critical insights into three-dimensional morphology, thickness evolution, pore structure, particle distribution, and structural uniformity, enabling a deeper understanding of reaction inhomogeneity and transport limitations.

Moreover, dry thick sulfur electrodes require integrated multiscale and multiphysics analysis. *Operando* Raman and *operando* XRD can track reaction intermediates and phase evolution, while *in situ* EIS probes interfacial and transport resistances, and tomography and SAXS capture structural evolution and pore network characteristics. Because structural and electrochemical inhomogeneities are amplified in thick

electrodes, experimental observations alone may not fully describe reaction mechanisms. Therefore, future studies should combine experimental analysis with multiscale modeling to elucidate the interactions among structure, reaction, and transport, and to systematically understand the impact of electrode design parameters on battery performance.

CONCLUSION AND OUTLOOK

High sulfur loading is essential for achieving practical high-energy-density LSBs. This review systematically summarizes recent research trends on key design elements for dry thick sulfur cathodes, including control of electronic and ionic transport, structural stabilization, and suppression of the polysulfide shuttle. In addition, structural and processing strategies applicable to LSB systems have been proposed based on dry thick electrode studies reported for LIB systems. This review further discusses operando and *in situ* electrochemical analyses, as well as microstructural characterization techniques, for directly investigating reaction mechanisms and structural evolution in thick electrodes. Through integrated interpretation of these analyses, such approaches will play a critical role in the mechanism-based design and optimization of dry thick sulfur cathodes.

Moving forward, dry thick sulfur cathodes should be developed to simultaneously meet practical requirements such as high sulfur loading and lean electrolyte conditions. Although many studies have demonstrated the feasibility of dry processing, most remain limited to relatively low sulfur loadings and therefore do not fully realize the advantages of dry thick electrodes. Accordingly, practical cell designs must achieve high sulfur loading, high sulfur utilization, high sulfur fraction, low E/S ratio, and low N/P ratio, while maintaining stable electrochemical performance at the pouch-cell level. To this end, the following strategies should be explored.

(1) *Materials exploration and design strategies*

Sulfur/carbon conductive composites are fundamental materials for thick sulfur cathodes. For practical applications, increasing sulfur content is necessary; however, the fraction of conductive additives cannot be increased indefinitely, and the carbon structure must provide both sufficient electronic conductivity and polysulfide accommodation. Therefore, hierarchical pore design that integrates micropores for sulfur confinement, mesopores for electrolyte accessibility, and macropores for transport is critical. During the first discharge, sulfur undergoes approximately an 80% volume expansion, which can compromise electrode structural integrity. In this regard, the use of prelithiated sulfur, such as Li_2S, as the initial active material may offer advantages, as the volume contraction during the first charge can generate additional porosity within the electrode[113,114]. This can alleviate the issue of low initial porosity in dry dense electrodes and facilitate electrolyte infiltration, representing a viable research direction. Moreover, such strategies may enable extension to anode-free cell configurations, offering potential for ultrahigh-energy-density cell design.

The design of conductive additives serves as a critical factor governing both electronic transport and structural stability in thick sulfur cathodes. Recent studies in dry thick LIB electrodes have shown that porosity and electrical conductivity vary depending on the type and morphology of conductive additives[115]. In thick sulfur cathodes, conductive materials that exhibit strong interactions with sulfur hosts and form stable conductive networks are required. In particular, when the size and morphology of conductive additives are comparable to those of sulfur/carbon composite hosts, more uniform dispersion and effective percolation network formation may be achieved. In addition, combining multiple conductive materials, such as carbon black, CNTs, graphene, and carbon fibers, to form multiscale percolation networks can be an effective strategy. Furthermore, to overcome the limitations of nonpolar carbon surfaces, surface modification via the introduction of polar functional groups or heteroatom doping can enhance interactions

with sulfur species and polysulfides. Designing conductive additives that enhance interfacial binding to binder fibril structures may also help achieve stable electrode architectures.

Binders are key components governing mechanical stability, microstructural integrity, electrolyte wetting, and even shuttle suppression. Practical binders for dry thick sulfur electrodes should go beyond simple adhesion and fulfill three essential functions. First, they should provide a balance between mechanical strength and flexibility to accommodate repeated stress associated with sulfur volume changes. Second, they should form stable interfacial bonding with conductive additives and sulfur to minimize contact loss during cycling. Third, they should enable uniform reaction behavior through interactions with polysulfides or enhanced electrolyte affinity. While PTFE fibrillation is widely used in dry processes, PTFE is nonpolar and exhibits low ionic affinity, which can result in poor wetting despite its robust mechanical network formation. Therefore, future binder design should focus on fiber-forming binders, composite binders, or dual-binder systems that simultaneously provide mechanical integrity and interfacial functionality.

Catalysts and functional additives play critical roles in improving sulfur utilization, suppressing polysulfide shuttle, and enhancing electrolyte wetting in thick sulfur cathodes. Sulfur redox kinetics become more important in thick electrodes due to increased reaction inhomogeneity with electrode thickness[116]. Therefore, catalysts should facilitate uniform sulfur redox reactions throughout the electrode and mitigate the shuttle effect. Although various sulfur catalysts have been reported, relatively few studies have demonstrated their effectiveness under practical conditions involving high sulfur loading and lean electrolyte. Thus, structural design and dispersion strategies that maintain catalytic functionality under practical conditions are required. In addition, under high-density and lean electrolyte conditions, infiltration of the electrolyte into the electrode may be limited. Therefore, the uniform dispersion of electrolyte-philic additives within the electrode can improve electrolyte infiltration and ionic transport.

(2) *Development of dry processes for thick sulfur electrodes*

To achieve high-energy-density and high-stability thick sulfur electrodes, processing strategies must be further developed considering LSB-specific characteristics. For example, in powder compression processes, excessive pressure may collapse the pore structure of the sulfur host and limit electrolyte infiltration; therefore, optimization of the trade-off between pressure and porosity is required. Similarly, in hot pressing, the dissolution and volatilization of sulfur should be carefully considered. In binder fibrillation-based processes, incorporating auxiliary binders with electrolyte affinity or shuttle-suppressing properties may be an effective strategy. Meanwhile, powder spray processes can control both ionic and electronic pathways while also enabling interlayer-like functionalities, such as the formation of a polar additive- or catalyst-rich sulfur-conductive composite layer near the separator, which can contribute to shuttle suppression.

In addition, in practical high-loading, thick-sulfur electrodes, the electrolyte infiltration process becomes a critical manufacturing parameter. Unlike wet-based processes, dry electrodes lack solvent-driven self-distribution effects; therefore, insufficient wetting after electrolyte injection may result in partial electrode activation, with only certain regions participating in reactions. Accordingly, processing strategies such as controlling electrolyte injection rate, vacuum infiltration, pre-wetting treatments, and electrolyte viscosity should be considered. In particular, under low E/S conditions, uniform distribution of a limited amount of electrolyte throughout the electrode directly affects sulfur utilization and reaction uniformity, making precise process control critical.

(3) *Lithium anode design*

Lithium metal anodes paired with dry thick sulfur cathodes should be designed with consideration of both Li utilization and interfacial stability under practical operating conditions. Sulfur cathodes operate as discharge-initiated lithium metal batteries, where the reaction begins with lithium stripping. Under high sulfur loading and low N/P conditions, increased Li utilization can lead to localized stripping hotspots and pit formation[117]. Pit formation results in fresh Li exposure, non-uniform SEI formation, Li pulverization, dead Li accumulation, and electrolyte depletion, all of which accelerate degradation in thick sulfur cathodes. In particular, under lean electrolyte conditions, repeated formation and breakdown of SEI continuously consume electrolyte, leading to increased internal resistance and Li depletion. Under high-current-density conditions in high-loading electrodes, pit-free stripping and stable SEI formation are critical. Strategies such as the removal and homogenization of the native oxide layer on Li metal, the formation of a LiF-rich artificial SEI, polymer/ceramic hybrid coatings, and the use of 3D current collectors to reduce local current density can be employed. In addition, bulk structural engineering approaches, such as crystallographic texture control, composite Li metal, and porous host structures, can promote uniform stripping and plating[118]. Ultimately, Li metal design strategies that simultaneously consider Li inventory balance and interfacial stability under high-sulfur loading, low E/S, and low N/P conditions are required.

(4) *Electrolyte engineering*

In thick electrodes with limited electrolyte infiltration and ionic transport, electrolyte properties and composition critically influence overall electrode performance. However, the requirements for electrolyte design differ substantially depending on the sulfur reaction pathway. In liquid polysulfide-mediated systems, electrolyte design must balance LiPS solubility, viscosity, wettability, ionic conductivity, and shuttle suppression[119,120]. Under lean electrolyte conditions, a limited amount of electrolyte must support both sufficient Li-ion transport and polysulfide reactions[121]. Low-viscosity electrolytes generally provide rapid infiltration and good wetting, enabling more uniform reactions even in thick electrodes. However, they may also promote excessive dissolution and diffusion of LiPS, thereby exacerbating the shuttle effect. In contrast, high-concentration electrolytes (HCEs) can suppress LiPS solubility and mobility by modifying the solvation structure, thereby stabilizing the reaction environment, although their increased viscosity may limit infiltration into thick electrodes. However, in solid-conversion-dominated sulfur systems, where polysulfide dissolution is intentionally suppressed, electrolyte design should focus less on promoting LiPS solubility and more on maintaining interfacial stability, ionic accessibility, and effective charge transfer at the sulfur/carbon/electrolyte interfaces[122,123].

Therefore, electrolyte design for thick sulfur electrodes should be tailored to the dominant reaction mechanism rather than treated as a universal strategy. For liquid polysulfide systems, localized high-concentration electrolytes can maintain locally high-concentration characteristics while reducing viscosity compared to conventional HCEs, thereby improving infiltration. Alternatively, low-viscosity solvents combined with additives that regulate LiPS interactions may be employed. For solid-conversion-type systems, electrolyte and electrode design should instead prioritize intimate interfacial contact, stable ion-conducting pathways, and suppression of inactive sulfur domains. Ultimately, achieving high-energy-density LSBs requires electrolyte design that simultaneously addresses infiltration, transport, and reaction-mechanism-specific sulfur regulation.

DECLARATIONS

Authors' contributions

Writing-original draft: Jeong, Y. H.; Jung, G.
Writing-review and editing: Jeong, Y. H.; Jung, G.
Collecting and analyzing: Jeong, Y. H.; Jung, G.
Supervision: Jo, C.
Funding acquisition: Jo, C.

Availability of data and materials

Not applicable.

AI and AI-assisted tools Statement

Not applicable.

Financial support and sponsorship

This work was supported by the research fund of Korea Institute of Materials Science (PNKB230) and the National Research Foundation of Korea (NRF) grant funded by the Korea government (MSIT) (No.RS-2025-25441256)

Conflicts of interest

Not applicable.

Ethical approval and consent to participate

Not applicable.

Consent for publication

Not applicable.

REFERENCES

1. Liu, J.; Bao, Z.; Cui, Y.; et al. Pathways for practical high-energy long-cycling lithium metal batteries. *Nat. Energy.* **2019**, *4*, 180-6. DOI
2. Zhou, G.; Chen, H.; Cui, Y. Formulating energy density for designing practical lithium–sulfur batteries. *Nat. Energy.* **2022**, *7*, 312-9. DOI
3. Wild, M.; O'Neill, L.; Zhang, T.; et al. Lithium sulfur batteries, a mechanistic review. *Energy. Environ. Sci.* **2015**, *8*, 3477-94. DOI
4. Guo, Y.; Niu, Q.; Pei, F.; et al. Interface engineering toward stable lithium-sulfur batteries. *Energy. Environ. Sci.* **2024**, *17*, 1330-67. DOI
5. Fei, Y.; Li, G. Unveiling the pivotal parameters for advancing high energy density in lithium-sulfur batteries: a comprehensive review. *Adv. Funct. Mater.* **2024**, *34*, 2312550. DOI
6. Wang, K.; Ma, Y.; Brezesinski, T.; Ma, Y.; Wu, Y. Fast reaction kinetics via interfacial mediation in quasi- and all-solid-state lithium-sulfur batteries. *Research* **2025**, *8*, 0949. DOI PubMed PMC
7. Xia, S.; Yan, L.; Wang, N.; et al. $Li_{0.95}Na_{0.05}FePO_4$ as a trifunctional additive to boost the electrochemical performance of cathodes in lithium-sulfur batteries. *EES. Batteries.* **2026**, *2*, 130-7. DOI
8. Saroha, R.; Lee, J. S.; Cho, S. W.; Cho, C.; Park, J.; Cho, J. S. Polysulfide barrier comprising bismuth selenide nanocrystals well anchored within N-doped carbon microspheres for stable Li-S batteries. *Energy. Mater.* **2025**, *5*, 500089. DOI
9. Manthiram, A.; Fu, Y.; Su, Y. Challenges and prospects of lithium-sulfur batteries. *Acc. Chem. Res.* **2012**, *46*, 1125-34. DOI
10. Yao, W.; Liao, K.; Lai, T.; Sul, H.; Manthiram, A. Rechargeable metal-sulfur batteries: key materials to mechanisms. *Chem. Rev.* **2024**, *124*, 4935-5118. DOI
11. Ke, J.; Wang, Z.; Zhu, H.; et al. Suppression strategies for the polysulfide shuttle effect in electrolyte systems. *Commun. Mater.* **2025**, *6*, 237. DOI
12. Shanghai Metals Market Home Page. https://www.metal.com/. (accessed 2026-06-24).
13. Suess, H. E.; Urey, H. C. Abundances of the elements. *Rev. Mod. Phys.* **1956**, *28*, 53-74. DOI
14. Dutch, S. I. Periodic tables of elemental abundance. *J. Chem. Educ.* **1999**, *76*, 356. DOI
15. Zhou, F.; Wu, Q.; Meng, J.; Xu, J.; Cao, F. Rare-earth-based strategies for lithium-sulfur batteries: enhancing multi-electron conversion reaction kinetics. *Energy. Z.* **2025**, *1*, 10002. DOI
16. Son, D.; Lim, W.; Lee, J. A short review of the recent developments in functional separators for lithium-sulfur batteries. *Korean. J. Chem. Eng.* **2023**, *40*, 473-87. DOI
17. Seh, Z. W.; Sun, Y.; Zhang, Q.; Cui, Y. Designing high-energy lithium-sulfur batteries. *Chem. Soc. Rev.* **2016**, *45*, 5605-34. DOI
18. Bi, C. X.; Zhao, M.; Hou, L. P.; et al. Anode material options toward 500 Wh kg^{-1} lithium-sulfur batteries. *Adv. Sci.* **2021**, *9*, 2103910. DOI

19. Bi, C.; Hou, L.; Li, Z.; et al. Protecting lithium metal anodes in lithium-sulfur batteries: a review. *Energy. Mater. Adv.* **2023**, *4*, 0010. DOI
20. Dörfler, S.; Althues, H.; Härtel, P.; Abendroth, T.; Schumm, B.; Kaskel, S. Challenges and key parameters of lithium-sulfur batteries on pouch cell level. *Joule* **2020**, *4*, 539-54. DOI
21. Shi, L.; Bak, S.; Shadike, Z.; et al. Reaction heterogeneity in practical high-energy lithium–sulfur pouch cells. *Energy. Environ. Sci.* **2020**, *13*, 3620-32. DOI
22. Chen, Z. X.; Zhao, M.; Hou, L. P.; Zhang, X. Q.; Li, B. Q.; Huang, J. Q. Toward practical high-energy-density lithium-sulfur pouch cells: a review. *Adv. Mater.* **2022**, *34*, 2201555. DOI
23. Kong, L.; Jin, Q.; Huang, J. Q.; et al. Nonuniform redistribution of sulfur and lithium upon cycling: probing the origin of capacity fading in lithium-sulfur pouch cells. *Energy. Tech.* **2019**, *7*, 1900111. DOI
24. Betz, J.; Bieker, G.; Meister, P.; Placke, T.; Winter, M.; Schmuch, R. Theoretical versus practical energy: a plea for more transparency in the energy calculation of different rechargeable battery systems. *Adv. Energy. Mater.* **2018**, *9*, 1803170. DOI
25. Wang, M.; Bai, Z.; Yang, T.; et al. Advances in high sulfur loading cathodes for practical lithium-sulfur batteries. *Adv. Energy. Mater.* **2022**, *12*, 2201585. DOI
26. Li, Z.; Sami, I.; Yang, J.; Li, J.; Kumar, R. V.; Chhowalla, M. Lithiated metallic molybdenum disulfide nanosheets for high-performance lithium-sulfur batteries. *Nat. Energy.* **2023**, *8*, 84-93. DOI
27. Guo, Y.; Jin, Z.; Lu, J.; et al. Engineering a deficient-coordinated single-atom indium electrocatalyst for fast redox conversion in practical 500 W h kg^{-1}-level pouch lithium-sulfur batteries. *Energy. Environ. Sci.* **2023**, *16*, 5274-83. DOI
28. Guo, J.; Liang, H.; Yang, Q.; et al. Steric-hindrance effect induced fabrication of lightweight, Bi-functional, and easy-to-infiltrate hosts for 502 Wh kg^{-1} lithium-sulfur batteries. *Adv. Mater.* **2025**, *38*, e18154. DOI
29. Kim, S.; Lim, W.; Jung, H.; et al. Protective catalytic layer powering activity and stability of electrocatalyst for high-energy lithium-sulfur pouch cell. *Nat. Commun.* **2025**, *16*, 1649. DOI PubMed PMC
30. Ji, X.; Lee, K. T.; Nazar, L. F. A highly ordered nanostructured carbon-sulphur cathode for lithium-sulphur batteries. *Nat. Mater.* **2009**, *8*, 500-6. DOI
31. Wei Seh, Z.; Li, W.; Cha, J. J.; et al. Sulphur-TiO_2 yolk-shell nanoarchitecture with internal void space for long-cycle lithium-sulphur batteries. *Nat. Commun.* **2013**, *4*, 1331. DOI
32. Babu, G.; Ababtain, K.; Ng, K. Y. S.; Arava, L. M. R. Electrocatalysis of lithium polysulfides: current collectors as electrodes in Li/S battery configuration. *Sci. Rep.* **2015**, *5*, 8763. DOI PubMed PMC
33. Peng, H. J.; Huang, J. Q.; Cheng, X. B.; Zhang, Q. Review on high-loading and high-energy lithium-sulfur batteries. *Adv. Energy. Mater.* **2017**, *7*, 1700260. DOI
34. Kuang, Y.; Chen, C.; Kirsch, D.; Hu, L. Thick electrode batteries: principles, opportunities, and challenges. *Adv. Energy. Mater.* **2019**, *9*, 1901457. DOI
35. Lampkin, J.; Li, H.; Furness, L.; Raccichini, R.; Garcia-Araez, N. A critical evaluation of the effect of electrode thickness and side reactions on electrolytes for aluminum-sulfur batteries. *ChemSusChem* **2020**, *13*, 3514-23. DOI
36. Shao, J.; Zheng, J.; Xing, G.; Lu, Y.; Lv, X.; Zhang, C. Design and preparation of thick electrodes for lithium-ion batteries. *J. Energy. Storage.* **2024**, *103*, 114357. DOI
37. Kumberg, J.; Müller, M.; Diehm, R.; et al. Drying of lithium-ion battery anodes for use in high-energy cells: influence of electrode thickness on drying time, adhesion, and crack formation. *Energy. Tech.* **2019**, *7*, 1900722. DOI
38. Yu, J.; Kim, B.; Yoo, Y. Dry electrode processing for lithium-ion battery cathodes and anodes: materials, fabrication strategies, and future outlook. *Adv. Mater. Technol.* **2025**, *10*, e01420. DOI
39. Ahmed, S.; Nelson, P. A.; Gallagher, K. G.; Dees, D. W. Energy impact of cathode drying and solvent recovery during lithium-ion battery manufacturing. *J. Power. Sources.* **2016**, *322*, 169-78. DOI
40. Yuan, C.; Deng, Y.; Li, T.; Yang, F. Manufacturing energy analysis of lithium ion battery pack for electric vehicles. *CIRP. Annals.* **2017**, *66*, 53-6. DOI
41. Sul, H.; Lee, D.; Manthiram, A. Highloading lithium-sulfur batteries with solvent-free dry-electrode processing. *Small* **2024**, *20*, 2400728. DOI
42. Suh, Y.; Koo, J. K.; Im, H.; Kim, Y. Astonishing performance improvements of dry-film graphite anode for reliable lithium-ion batteries. *Chem. Eng. J.* **2023**, *476*, 146299. DOI
43. Hong, T. H.; Kim, D. J.; Ko, S. M.; Lee, J. T. Solvent-free dry-process for developing high-performance lithium-sulfur batteries. *Korean. J. Chem. Eng.* **2025**, *42*, 1475-90. DOI
44. Park, H.; Jin, C.; Daniel, C.; Li, J. Dry-processed electrodes enabled by polytetrafluoroethylene fibrillation for high-performance lithium-ion batteries. *Progress. Mater. Sci.* **2026**, *160*, 101674. DOI

45. Ardakani, H. A.; Mitsoulis, E.; Hatzikiriakos, S. G. Polytetrafluoroethylene paste extrusion: a fibrillation model and its relation to mechanical properties. *Int. Polym. Process.* **2013**, *28*, 306-13. DOI
46. Sudhakaran, S.; Bijoy, T. K. A comprehensive review of current and emerging binder technologies for energy storage applications. *ACS. Appl. Energy. Mater.* **2023**, *6*, 11773-94. DOI
47. Oh, H.; Kim, G.; Hwang, B. U.; Bang, J.; Kim, J.; Jeong, K. Development of a feasible and scalable manufacturing method for PTFE-based solvent-free lithium-ion battery electrodes. *Chem. Eng. J.* **2024**, *491*, 151957. DOI
48. Hong, J.; Yoon, J.; Park, J.; Ha, Y.; Lee, J.; Hwang, I. Optimization of PTFE fibrillation in dry electrode process for scalable all-solid-state battery manufacturing. *J. Power. Sources.* **2025**, *655*, 237925. DOI
49. Bouguern, M. D.; Madikere Raghunatha Reddy, A. K.; Li, X.; Deng, S.; Laryea, H.; Zaghib, K. Engineering dry electrode manufacturing for sustainable lithium-ion batteries. *Batteries* **2024**, *10*, 39. DOI
50. Park, J.; Kim, J.; Kim, J.; Kim, M.; Song, T.; Paik, U. Sustainable and cost-effective electrode manufacturing for advanced lithium batteries: the roll-to-roll dry coating process. *Chem. Sci.* **2025**, *16*, 6598-619. DOI PubMed PMC
51. Zhao, M.; Li, B.; Zhang, X.; Huang, J.; Zhang, Q. A perspective toward practical lithium-sulfur batteries. *ACS. Cent. Sci.* **2020**, *6*, 1095-104. DOI
52. Wang, D.; Wen, C.; Li, R.; et al. Point-line hybrid percolation conductive carbon networks in composite electrodes for high-power and durable aqueous Zn-V battery. *Carbon* **2026**, *254*, 121517. DOI
53. Lee, E.; Lee, D.; Bessette, S.; et al. Nearly all-active-material cathodes free of nickel and cobalt for Li-ion batteries. *Energy. Environ. Sci.* **2024**, *17*, 3753-64. DOI
54. Oh, J.; Kim, J.; Lim, J.; Park, K.; Yoon, S.; Jo, C. Incorporation of high-valence dopants in primary particles for strain-resistive Co-free high-Ni $LiNi_{0.9}Mn_{0.1}O_2$ cathodes. *Mater. Today.* **2025**, *88*, 314-21. DOI
55. Park, S.; Kim, D. R.; Choe, G.; et al. Engineering homogeneous dopant distribution via nano-sol infusion: a strategy for microcrack suppression in $LiNiO_2$. *Small* **2026**, *22*, e00001. DOI
56. Li, G.; Wang, S.; Zhang, Y.; Li, M.; Chen, Z.; Lu, J. Revisiting the role of polysulfides in lithium-sulfur batteries. *Adv. Mater.* **2018**, *30*, 1705590. DOI
57. Huang, C.; Cheng, J.; Su, W.; et al. Origin of shuttle-free sulfurized polyacrylonitrile in lithium-sulfur batteries. *J. Power. Sources.* **2021**, *492*, 229508. DOI
58. Lee, D.; Kim, Y.; Shin, M. The role of stack pressure in modulating electrochemical behavior of all-solid-state lithium-sulfur batteries. *Korean. J. Chem. Eng.* **2025**, *42*, 1507-15. DOI
59. Yang, Y.; Liu, C.; Su, M.; et al. Kinetic mechanism and structural design of thick electrodes in lithium-ion batteries: challenges and optimization strategies. *Small* **2025**, *21*, e06931. DOI
60. Kohl, M.; Brückner, J.; Bauer, I.; Althues, H.; Kaskel, S. Synthesis of highly electrochemically active Li_2S nanoparticles for lithium-sulfur-batteries. *J. Mater. Chem. A.* **2015**, *3*, 16307-12. DOI
61. Strubel, P.; Thieme, S.; Biemelt, T.; et al. ZnO hard templating for synthesis of hierarchical porous carbons with tailored porosity and high performance in lithium-sulfur battery. *Adv. Funct. Mater.* **2014**, *25*, 287-97. DOI
62. Cronk, A.; Wang, X.; Oh, J. A. S.; et al. A highly utilized and practical lithium-sulfur positive electrode enabled in all-solid-state batteries. *Nat. Commun.* **2026**, *17*, 3298. DOI PubMed PMC
63. Kim, D. J.; Hong, T. H.; Lee, J. S.; et al. Solvent-free dry-process enabling high-areal loading selenium-doped SPAN cathodes toward practical lithium-sulfur batteries. *Small* **2025**, *21*, 2503037. DOI
64. Horst, M.; Burmeister, J. K.; Abdollahifar, M.; Pillitteri, S.; Kwade, A. A binder-free dry coating process for high sulfur loading cathodes of Li-S batteries: a proof-of-concept. *J. Power. Sources.* **2023**, *587*, 233675. DOI
65. Kim, H.; Hwang, J.; Bang, S.; Jung, H.; Sun, Y. Geometrical engineering of a SPAN-graphene composite cathode for practical Li-S batteries. *J. Mater. Chem. A.* **2022**, *10*, 10844-53. DOI
66. Lin, Y.; Jones, K. J.; Greenburg, L. C.; Kim, J. W.; Hu, L.; Connell, J. W. Facile, solvent-free preparation of high density, high mass loading sulfur cathodes enabled by dry-pressable holey graphene scaffolds. *Batteries. Supercaps.* **2019**, *2*, 774-83. DOI
67. Zuluaga-Gómez, C. C.; Plaza-Rivera, C. O.; Tripathi, B.; et al. Holey graphene/ferroelectric/sulfur composite cathodes for high-capacity lithium-sulfur batteries. *ACS. Omega.* **2023**, *8*, 13097-108. DOI
68. Wang, D.; Jhang, L.; Kou, R.; et al. Realizing high-capacity all-solid-state lithium-sulfur batteries using a low-density inorganic solid-state electrolyte. *Nat. Commun.* **2023**, *14*, 1895. DOI PubMed PMC
69. Lv, Z.; Liu, J.; Li, C.; et al. High-areal-capacity all-solid-state Li-S battery enabled by dry process technology. *eTransportation* **2024**, *19*, 100298. DOI
70. Chen, S.; Du, G.; Cheng, Y.; et al. Dry-processing of VN quantum dots/N, O, S-doped hierarchical porous carbon electrodes with high sulfur-loading for practical lithium-sulfur batteries. *Chem. Eng. J.* **2025**, *509*, 161440. DOI

71. Dörfler, S.; Strubel, P.; Jaumann, T.; et al. On the mechanistic role of nitrogen-doped carbon cathodes in lithium-sulfur batteries with low electrolyte weight portion. *Nano. Energy.* **2018**, *54*, 116-28. DOI
72. Zuluaga-Gómez, C. C.; Tripathi, B.; Plaza-Rivera, C. O.; et al. High areal capacity and sustainable high energy in ferroelectric doped holey graphene/sulfur composite cathode for lithium-sulfur batteries. *Batteries* **2023**, *9*, 293. DOI
73. Guo, R.; Yang, Y.; Huang, X. L.; et al. Recent advances in multifunctional binders for high sulfur loading lithium-sulfur batteries. *Adv. Funct. Mater.* **2023**, *34*, 2307108. DOI
74. Yang, Y.; Zheng, G.; Misra, S.; Nelson, J.; Toney, M. F.; Cui, Y. High-capacity micrometer-sized Li_2S particles as cathode materials for advanced rechargeable lithium-ion batteries. *J. Am. Chem. Soc.* **2012**, *134*, 15387-94. DOI
75. Su, D.; Zhou, D.; Wang, C.; Wang, G. Toward high performance lithium-sulfur batteries based on Li_2S cathodes and beyond: status, challenges, and perspectives. *Adv. Funct. Mater.* **2018**, *28*, 1800154. DOI
76. Liu, G.; Chen, T.; Chung, C.; Lin, H.; Hsu, C. Hierarchical micro/mesoporous carbons synthesized with a ZnO template and petroleum pitch via a solvent-free process for a high-performance supercapacitor. *ACS. Omega.* **2017**, *2*, 2106-13. DOI PubMed PMC
77. Kim, W.; Jang, D.; Kim, H. Understanding electronic and Li-ion transport of $LiNi_{0.5}Co_{0.2}Mn_{0.3}O_2$ electrodes affected by porosity and electrolytes using electrochemical impedance spectroscopy. *J. Power. Sources.* **2021**, *510*, 230338. DOI
78. Ohno, S.; Zeier, W. G. Toward practical solid-state lithium-sulfur batteries: challenges and perspectives. *Acc. Mater. Res.* **2021**, *2*, 869-80. DOI
79. Camacho-Forero, L. E.; Balbuena, P. B. Elucidating interfacial phenomena between solid-state electrolytes and the sulfur-cathode of lithium-sulfur batteries. *Chem. Mater.* **2019**, *32*, 360-73. DOI
80. Kumano, N.; Yamaguchi, Y.; Akimoto, Y.; Ohshima, A.; Nakamura, H.; Yamamura, M. Migration of binder and conductive agent during drying process of Li-ion battery cathodes. *J. Power. Sources.* **2024**, *591*, 233883. DOI
81. Jang, Y.; Lee, S.; Lee, Y.; et al. Sieve-assisted fabrication of NCM622 dry electrodes with enhanced interfacial adhesion. *J. Power. Sources.* **2026**, *663*, 238739. DOI
82. Zhu, X.; Wang, L.; Bai, Z.; Lu, J.; Wu, T. Sulfide-based all-solid-state lithium–sulfur batteries: challenges and perspectives. *Nano-Micro. Lett.* **2023**, *15*, 75. DOI PubMed PMC
83. Du, M.; Hao, Z.; Liu, Y.; et al. Architecture engineering for thick electrodes in high-energy batteries: challenges and strategies. *ACS. Appl. Mater. Interfaces.* **2025**, *17*, 19230-46. DOI
84. Kim, J.; Kim, M.; Han, S.; Paik, U.; Song, T. Development of nano-sized $LiFePO_4$ dry cathodes with enhanced flexibility and mechanical robustness for roll-to-roll dry coating process. *Microstructures* **2026**, *6*, 2026044. DOI
85. Heary, R. F.; Parvathreddy, N.; Sampath, S.; Agarwal, N. Elastic modulus in the selection of interbody implants. *J. Spine. Surg.* **2017**, *3*, 163-7. DOI PubMed PMC
86. Fiedler, M.; Cangaz, S.; Hippauf, F.; et al. Mechanistic insights into the cycling behavior of sulfur dry-film cathodes. *Adv. Sustain.* **2023**, *7*, 2200439. DOI
87. Lu, Y.; Zhao, M.; Yang, Y.; et al. A conductive framework embedded with cobalt-doped vanadium nitride as an efficient polysulfide adsorber and convertor for advanced lithium-sulfur batteries. *Nanoscale. Horiz.* **2022**, *7*, 543-53. DOI
88. Li, C.; Xi, Z.; Guo, D.; Chen, X.; Yin, L. Chemical immobilization effect on lithium polysulfides for lithium-sulfur batteries. *Small* **2017**, *14*, 1701986. DOI
89. Yang, H.; Zhang, B.; Fan, D.; Zhao, X.; Li, F.; Zhang, C. Theoretical insights into 2D ferroelectric metal $CuZrP_2S_6$ for lithium-sulfur batteries: polarization modulation and the role of p doping. *J. Electron. Mater.* **2026**, *55*, 4031-42. DOI
90. Liu, Y.; Fang, P.; Wen, B.; Wu, X.; Zhang, L. Dry processing technique for high-energy density lithium batteries. *Small* **2025**, *21*, e10454. DOI
91. Park, S.; Shi, B.; Shang, Y.; Deng, K.; Fu, K. Structured electrode additive manufacturing for lithium-ion batteries. *Nano. Lett.* **2022**, *22*, 9462-9. DOI
92. Maurel, A.; Russo, R.; Grugeon, S.; Panier, S.; Dupont, L. Environmentally friendly lithium-terephthalate/polylactic acid composite filament formulation for lithium-ion Battery 3D-printing via fused deposition modeling. *ECS. J. Solid. State. Sci. Technol.* **2021**, *10*, 037004. DOI
93. Kang, J.; Eom, H.; Jang, S.; et al. Bollard-anchored binder system for high-loading cathodes fabricated via dry electrode process for Li-ion batteries. *Adv. Mater.* **2025**, *37*, 2416872. DOI
94. Gao, Y.; Yang, Y.; Yang, T.; et al. Design lithium exchanged zeolite based multifunctional electrode additive for ultra-high loading electrode toward high energy density lithium metal battery. *Adv. Energy. Mater.* **2024**, *15*, 2403063. DOI
95. Li, X.; Zhao, M.; Song, Y.; et al. Polysulfide chemistry in metal-sulfur batteries. *Chem. Soc. Rev.* **2025**, *54*, 4822-73. DOI
96. Zhang, Q.; Gao, S.; Yu, J. Metal sites in zeolites: synthesis, characterization, and catalysis. *Chem. Rev.* **2022**, *123*, 6039-106. DOI
97. Kang, X.; He, T.; Zou, R.; et al. Size effect for inhibiting polysulfides shuttle in lithium-sulfur batteries. *Small* **2023**, *20*, 2306503. DOI

98. Choi, J.; Polyzos, G.; Humphrey, H.; et al. Long carbon fibers boost performance of dry processed Li-ion battery electrodes. *J. Power. Sources.* **2025**, *640*, 236603. DOI
99. Kim, H. S.; Jung, J. Y.; Kim, K.; et al. Functionalized electrode additive for simultaneously reinforcing chemo-mechanical properties of millimeter-thick dry-electrode for high-energy all-solid-state batteries. *Adv. Energy. Mater.* **2023**, *14*, 2303965. DOI
100. Lee, T.; Kim, S.; Chung, W. J.; et al. Multifunctional liquefiable oligomer additive for dry electrode process. *ACS. Energy. Lett.* **2026**, *11*, 3496-505. DOI
101. Wang, M.; Md Pratik, S.; Nayir, N.; et al. Atomic-scale mechanistic insights into the ring-opening polymerization of elemental sulfur. *Angew. Chem. Int. Ed.* **2025**, *64*, e202511640. DOI
102. Sofekun, G. O.; Evoy, E.; Lesage, K. L.; Chou, N.; Marriott, R. A. The rheology of liquid elemental sulfur across the λ-transition. *J. Rheol.* **2018**, *62*, 469-76. DOI
103. Cuisinier, M.; Cabelguen, P.; Evers, S.; et al. Sulfur speciation in Li-S batteries determined by operando X-ray absorption spectroscopy. *J. Phys. Chem. Lett.* **2013**, *4*, 3227-32. DOI
104. Guo, Y.; Li, X.; Qin, Q.; et al. Determination of the tortuosity and contact resistances in thick graphite anodes via electrochemical impedance spectroscopy. *J. Power. Sources.* **2023**, *569*, 233003. DOI
105. Senol Gungor, A.; Von Mentlen, J.; Ruthes, J. G. A.; et al. Understanding rate and capacity limitations in Li-S batteries based on solid-state sulfur conversion in confinement. *ACS. Appl. Mater. Interfaces.* **2024**, *16*, 67651-61. DOI
106. Zhang, L.; Dai, Y.; Li, C.; et al. Recent advances in electrochemical impedance spectroscopy for solid-state batteries. *Energy. Storage. Mater.* **2024**, *69*, 103378. DOI
107. Schmidt, F.; Ehrling, S.; Schönherr, K.; et al. The importance of swelling effects on cathode density and electrochemical performance of lithium-sulfur battery cathodes produced via dry processing. *Energy. Tech.* **2021**, *10*, 2100721. DOI
108. Schmidt, F.; Fiedler, M.; Arlt, T.; et al. Impact of the carbon matrix composition on the S/C cathode porosity and performance in prototype Li-S cells. *Energy. Tech.* **2023**, *11*, 2300518. DOI
109. Watanabe, T.; Park, Y. J.; Yamamoto, K.; et al. Elucidation of the factors that determine the reaction distribution during charging in graphite electrodes for all-solid-state batteries using *in situ* nano X-ray tomography and digital volume correlation analysis. *ACS. Appl. Mater. Interfaces.* **2025**, *17*, 45704-12. DOI
110. Petzold, A.; Juhl, A.; Scholz, J.; et al. Distribution of sulfur in carbon/sulfur nanocomposites analyzed by small-angle X-ray scattering. *Langmuir* **2016**, *32*, 2780-6. DOI
111. Choi, Y. S.; Park, G. O.; Kim, K. H.; Kwon, Y.; Huh, J.; Kim, J. M. Unveiling the role of micropores in porous carbon for Li-S batteries using *operando* SAXS. *Chem. Commun.* **2021**, *57*, 10500-3. DOI
112. Tarimo, D. J.; García-soriano, F. J.; Vizintin, A.; Prehal, C.; Presser, V. Performance of microporous carbon cathodes and impact of cathode/solid electrolyte interphase formation using carbonate and ether-based electrolytes in lithium-sulfur batteries. *ACS. Appl. Energy. Mater.* **2025**, *8*, 12139-56. DOI
113. Hong, S.; Cao, Y.; Qi, J.; et al. High-valence-cation-induced lattice expansion for activating Li_2S cathode in all-solid-state lithium-sulfur batteries. *Adv. Mater.* **2026**, *38*, e72513. DOI
114. Jeong, Y. H.; Chung, G.; Park, G. H.; Kim, B. J.; Kim, W. B.; Jo, C. Electrochemical quantification of lithium oxide impurity in lithium sulfide via lithium-sulfur battery operation. *Anal. Chem.* **2025**, *97*, 24279-84. DOI
115. Oh, H.; Kim, G.; Bang, J.; Kim, S.; Jeong, K. Dry-processed thick electrode design with a porous conductive agent enabling 20 mA h cm^{-2} for high-energy-density lithium-ion batteries. *Energy. Environ. Sci.* **2025**, *18*, 645-58. DOI
116. Park, G. H.; Mangishetti, S. R.; Lim, W. G.; et al. Triphasic interface engineering with metallic Sn/N, B Co-doped carbon matrix for boosting reaction kinetics and cycling stability in lithium-sulfur batteries. *Small* **2025**, *21*, 2503534. DOI
117. Hong, Y. K.; Kim, H. D.; Choi, S.; et al. Pit-free stripping in discharge-initiated lithium metal batteries. *ACS. Energy. Lett.* **2026**, *11*, 2399-409. DOI
118. Kim, H.; Jo, C. Unraveling lithium metal plating behavior on cobalt-decorated 3D carbon textile for high-energy-density lithium metal batteries. *J. Energy. Chem.* **2026**, *114*, 264-76. DOI
119. Li, X.; Li, B.; Jin, T.; et al. Competitive anion coordination overcomes charge-transfer barriers for lithium-sulfur batteries. *Joule* **2026**, *10*, 102259. DOI
120. Xu, C.; Cheng, G.; Liu, S.; et al. Siloxane electrolyte molecular design for lithium-sulfur batteries. *Energy. Storage. Mater.* **2026**, *86*, 104970. DOI
121. Kang, T.; Kang, N.; Choi, J. W. Overview of highly solvating electrolytes for lean electrolyte conditions in lithium-sulfur batteries. *Korean. J. Chem. Eng.* **2024**, *41*, 375-83. DOI
122. Xu, W.; Mu, Y.; Yin, Y.; et al. Conjugated topologically confined composite electrolytes for robust high-voltage and high-temperature semi-solid-state lithium metal batteries. *Energy. Environ. Sci.* **2026**, *19*, 384-96. DOI

123. Zhang, X.; Hu, A.; He, M.; et al. Dual-scale steric-topological engineering of polymer electrolytes for solid-state lithium metal batteries. *Adv. Funct. Mater.* 2026, e74897. DOI